Materials Today Bio 28 (2024) 101174

Contents lists available at ScienceDirect

Materials Today Bio

journal homepage: www.journals.elsevier.com/materials-today-bio

A bioactive composite scaffold enhances osteochondral repair by using thermosensitive chitosan hydrogel and endothelial lineage cell-derived chondrogenic cell

Tzu-Hsiang Lin [a,b,d], Hsueh-Chun Wang [a], Yau-Lin Tseng [b,d], Ming-Long Yeh [a,c,*]

[a] Department of Biomedical Engineering, College of Engineering, National Cheng Kung University, 1 University Rd., Tainan, 701, Taiwan
[b] Department of Surgery, National Cheng Kung University Hospital, College of Medicine, National Cheng Kung University, 1 University Rd., Tainan, 701, Taiwan
[c] Innovation Headquarters, National Cheng Kung University, 1 University Rd., Tainan, 701, Taiwan
[d] Medical Imaging Center, National Cheng Kung University, 1 University Rd., Tainan, 701, Taiwan

ARTICLE INFO

Keywords:
Thermosensitive injectable hydrogels
Endothelial progenitor cells
Endothelial-to-mesenchymal transition
Chondrogenesis
Osteochondral regeneration

ABSTRACT

Articular cartilage regeneration is a major challenge in orthopedic medicine. Endothelial progenitor cells (EPCs) are a promising cell source for regenerative medicine applications. However, their roles and functions in cartilage regeneration are not well understood. Additionally, thermosensitive chitosan hydrogels have been widely used in tissue engineering, but further development of these hydrogels incorporating vascular lineage cells for cartilage repair is insufficient. Thus, this study aimed to characterize the ability of EPCs to undergo endothelial–mesenchymal stem cell transdifferentiation and chondrogenic differentiation and investigate the ability of chondrogenic EPC-seeded thermosensitive chitosan-graft-poly (*N*-isopropylacrylamide) (CEPC-CSPN) scaffolds to improve healing in a rabbit osteochondral defect (OCD) model. EPCs were isolated and endothelial-to-mesenchymal transition (EndMT) was induced by transforming growth factor-β1 (TGF-β1); these EPCs are subsequently termed transdifferentiated EPCs (tEPCs). The stem cell-like properties and chondrogenic potential of tEPCs were evaluated by a series of *in vitro* assays. Furthermore, the effect of CEPC-CSPN scaffolds on OCD repair was evaluated. Our *in vitro* results confirmed that treatment of EPC with TGF-β1 induced EndMT and the acquisition of stem cell-like properties, producing tEPCs. Upon inducing chondrogenic differentiation of tEPCs (CEPCs), the cells exhibited significantly enhanced chondrogenesis and chondrocyte surface markers after 25 days. The TGF-β1-induced differentiation of EPCs is mediated by both the TGF-β/Smad and extracellular signal-regulated kinase (Erk) pathways. The CEPC-CSPN scaffold reconstructed well-integrated translucent cartilage and repaired subchondral bone *in vivo*, exhibiting regenerative capacity. Collectively, our results suggest that the CEPC-CSPN scaffold induces OCD repair, representing a promising approach to articular cartilage regeneration.

1. Introduction

Osteochondral defects (OCDs) compromise the integrity and stability of the articular surface, leading to premature osteoarthritis. The successful regeneration of damaged articular cartilage remains an unmet challenge owing to its limited capacity for spontaneous repair. The emergence of cell-based cartilage tissue engineering offers distinct advantages over existing treatments for cartilage-related injuries.

Differentiated chondrocytes and bone marrow-derived mesenchymal stem cells (MSCs) are important cell sources for the treatment of cartilage-related injuries [1]. However, the limited proliferative capacity and dedifferentiation of chondrocytes, along with an insufficient supply of bone marrow-derived MSCs, present considerable challenges in transplantation and cartilage regeneration [2,3]. Furthermore, the

Abbreviations: BV/TV, bone volume per tissue volume; CEPCs, chondrogenic endothelial progenitor cells; CFU, colony forming unit; CSPN, chitosan-graft-poly(N-isopropylacrylamide); CEPC-CSPN, CSPN scaffold containing chondrogenic endothelial progenitor cells; eNOS, endothelial nitric oxide synthase; EPCs, endothelial progenitor cells; EndMT, endothelial-to-mesenchymal transition; EPC-CSPN, CSPN scaffold containing endothelial progenitor cells; LEPCs, late endothelial progenitor cells; MNC, mononuclear cell; MSCs, mesenchymal stem cells; sGAG, sulfated glycosaminoglycan; tEPCs, transdifferentiated EPCs; TGF-β, transforming growth factor-β; VE-cadherin, vascular endothelial cadherin.

* Corresponding author. Department of Biomedical Engineering, College of Engineering, National Cheng Kung University, 1 University Rd., Tainan, 701, Taiwan.
E-mail addresses: 10805025@gs.ncku.edu.tw (T.-H. Lin), mlyeh@mail.ncku.edu.tw (M.-L. Yeh).

https://doi.org/10.1016/j.mtbio.2024.101174
Received 21 May 2024; Received in revised form 19 July 2024; Accepted 29 July 2024
Available online 3 August 2024

harvesting of adult MSCs requires additional surgery. Endothelial progenitor cells (EPCs) are a promising alternative cell source for cartilage repair [4], as they can be obtained through minimally invasive techniques. Late EPCs (LEPCs) are an EPC subtype designated based on their time-dependent appearance and derived from adult peripheral blood. LEPCs have an endothelial-like cobblestone morphology, form distinct clusters, and have unlimited proliferative potential [5]. LEPCs express not only endothelial cell-specific markers (vascular endothelial [VE]-cadherin, kinase insert domain receptor, and von Willebrand factor [vWF]) but also the stem cell pluripotency marker, Oct-4 [6]. Studies showed that EPCs provide a microenvironment that induces the proliferation and differentiation of surrounding stem cells to repair OCDs [4,7]. However, evidence regarding the fate of transplanted EPCs is lacking. Whether EPCs transdifferentiate into MSCs and eventually differentiate into chondrocytes remains unclear. Thus, the transdifferentiation potential of EPCs may be a crucial factor for their application in tissue repair. Regarding cell transdifferentiation, reports indicated that endothelial cells can acquire a mesenchymal phenotype through endothelial-to-mesenchymal transition (EndMT) [8].

EndMT contributes to the development of several diseases by inducing morphological changes and pathological processes. EndMT generates various types of connective tissue [9], demonstrating its potential for tissue regeneration applications. EndMT transforms endothelial cells into MSCs, which differentiate into chondrocytes and osteoblasts using specific differentiation conditions [10,11]. EndMT is stimulated by various factors, including transforming growth factor (TGF)-β and the family of bone morphogenetic proteins of growth factors [12]. TGF-β1, a crucial cytokine for inducing MSC chondrogenesis [13] and maintaining the chondrocyte phenotype [14], is important for EndMT in endothelial cells [15]. TGF-β-induced EndMT is mediated via the canonical Smad pathway, with limited involvement of the non-canonical extracellular signal-regulated kinase (Erk) pathway [16]. The TGF-β/Smad and Erk pathways activate transcription factors (Snail/Twist) that inhibit endothelial gene expression and induce mesenchymal gene expression by inducing EndMT [17]. EPCs can undergo TGF-β/Smad-induced EndMT, gain mesenchymal marker expression, and transform into smooth muscle cells [18]. The versatility of EndMT offers potential for tissue repair applications in tissue engineering [19].

The thermosensitive polymer poly (*N*-isopropylacrylamide) is a popular material for tissue engineering applications. It is soluble in aqueous solutions below its lower critical solution temperature, above which it transforms into a solid hydrogel. Although its properties are essential for tissue regeneration, its application is hindered owing to its insufficient mechanical strength, biodegradability, and biocompatibility. However, it can be modified with chitosan or other natural polymers to facilitate biodegradation, strengthen its hydrogel mechanical properties, and enhance cell proliferation and differentiation. Using chitosan to develop cell-based materials for cartilage repair has several advantages, including biocompatibility, biodegradability, and ease of modification [20,21]. For example, chitosan-graft-poly (*N*-isopropylacrylamide) (CSPN) hydrogels have been shown to positively impact the morphology and viability of chondrocytes and meniscus cells [22] while also enhancing MSC chondrogenesis [23]. A recent study [24] demonstrated the efficacy of a novel CSPN hydrogel with good biodegradability, which provided sufficient mechanical support and created a suitable microenvironment for cell growth and the chondrogenic differentiation of pericartilage MSCs. The formulated CSPN hydrogel promoted cartilage regeneration and facilitated cartilage repair. CSPN hydrogels can also serve as injectable biocomposite carriers for delivering cells, mimicking *in vivo* conditions for culturing MSCs and chondrocytes. However, most studies have focused on the regenerative capacity of tissue-derived stem cells or mature chondrocytes incorporated into CSPN scaffolds. According to the findings of previous studies on cartilage repair [24–26], there is limited research regarding the effects of non-tissue-derived vascular cells in CSPN scaffolds and the long-term treatment of cartilage-related injuries using cell-seeded CSPN scaffolds.

In the current study, we aimed to characterize the ability of EPCs to undergo endothelial–mesenchymal stem cell transdifferentiation and chondrogenic differentiation and investigate the ability of chondrogenic EPC-seeded thermosensitive chitosan-graft-poly (*N*-isopropylacrylamide) (CEPC-CSPN) scaffolds to improve healing in a rabbit OCD model. Herein, CSPN scaffolds provided an optimal microenvironment conducive to cell growth, differentiation, and tissue regeneration. Non-tissue-derived EPCs were also stimulated with TGF-β1 to induce EndMT and MSC transformation and redifferentiated into chondrogenic EPCs (CEPCs) under chondrogenic stimuli. These CEPCs may function as a viable source of chondrocytes, providing biological cues that enhance the mobilization, proliferation, and differentiation of both stem cells and chondrocytes derived from pericartilage, thus facilitating the repair of damaged cartilage. Moreover, the integration of CEPCs with CSPN scaffolds could significantly improve the quality of repair tissue and promote the regeneration of functional osteochondral tissue. Widespread adoption of this strategy could lead to the development of innovative therapeutics for osteochondral regeneration. We anticipate that CEPC-seeded CSPN hydrogels would serve as a valuable platform for regenerative medicine.

2. Materials and methods

2.1. Materials

Food-grade chitosan (degree of deacetylation, 90 %; molecular weight = 3×10^5 Da) was obtained from Charming&Beauty (Dayuan, Taoyuan, Taiwan). N-isopropylacrylamide (NIPAAm), ammonium persulfate, and N,N,N′,N′-tetramethyl ethylene diamine (TEMED) were purchased from Sigma-Aldrich (St. Louis, MO, USA). All chemicals, except chitosan, were of analytical grade and used without further purification. Fetal bovine serum, Dulbecco's modified Eagle's medium, and antibiotics were purchased from Gibco BRL (Grand Island, NY, USA).

2.2. In vitro cell culture of rabbit EPCs (rEPCs)

2.2.1. Isolation and culture of rEPCs

The animal experimental protocol was approved by the National Cheng Kung University Animal Care and Use Committee (protocol number: 104264). Peripheral blood (10 mL/kg) was obtained from New Zealand white rabbits through the peripheral ear artery. Peripheral blood mononuclear cells were isolated via density gradient centrifugation using Ficoll-Plaque® Plus (Amersham Biosciences, Amersham, Buckinghamshire, UK). Subsequently, the mononuclear cells were washed, incubated in 6-well culture plates coated with fibronectin, and supplemented with endothelial growth medium-2 (Cambrex Corp., East Rutherford, NJ, USA), comprising endothelial basal medium, 5 % fetal bovine serum, human epidermal growth factor, vascular endothelial growth factor, human fibroblastic growth factor-B, insulin-like growth factor-1, ascorbic acid, and heparin. After 28 days of incubation, the adherent cells (LEPCs) were harvested through trypsinization for subsequent cytokine induction, analysis, or transplantation (Fig. 1a). The characterization and confirmation of EPCs isolated from rabbits were conducted as described previously [27].

2.3. Induction of EndMT and cell differentiation in cultured rEPCs

2.3.1. EndMT induction and tri-lineage differentiation of rEPCs

Briefly, LEPCs in passages 2–5 were cultured and expanded as monolayers in endothelial growth medium-2 at 37 °C in an atmosphere containing 5 % CO_2. Upon reaching ~80 % confluency, LEPCs were treated with 10 ng/mL TGF-β1 (Thermo Fisher Scientific, Waltham, MA, USA) for 7 days to induce EndMT (Fig. 1a). After 7 days of culture, we

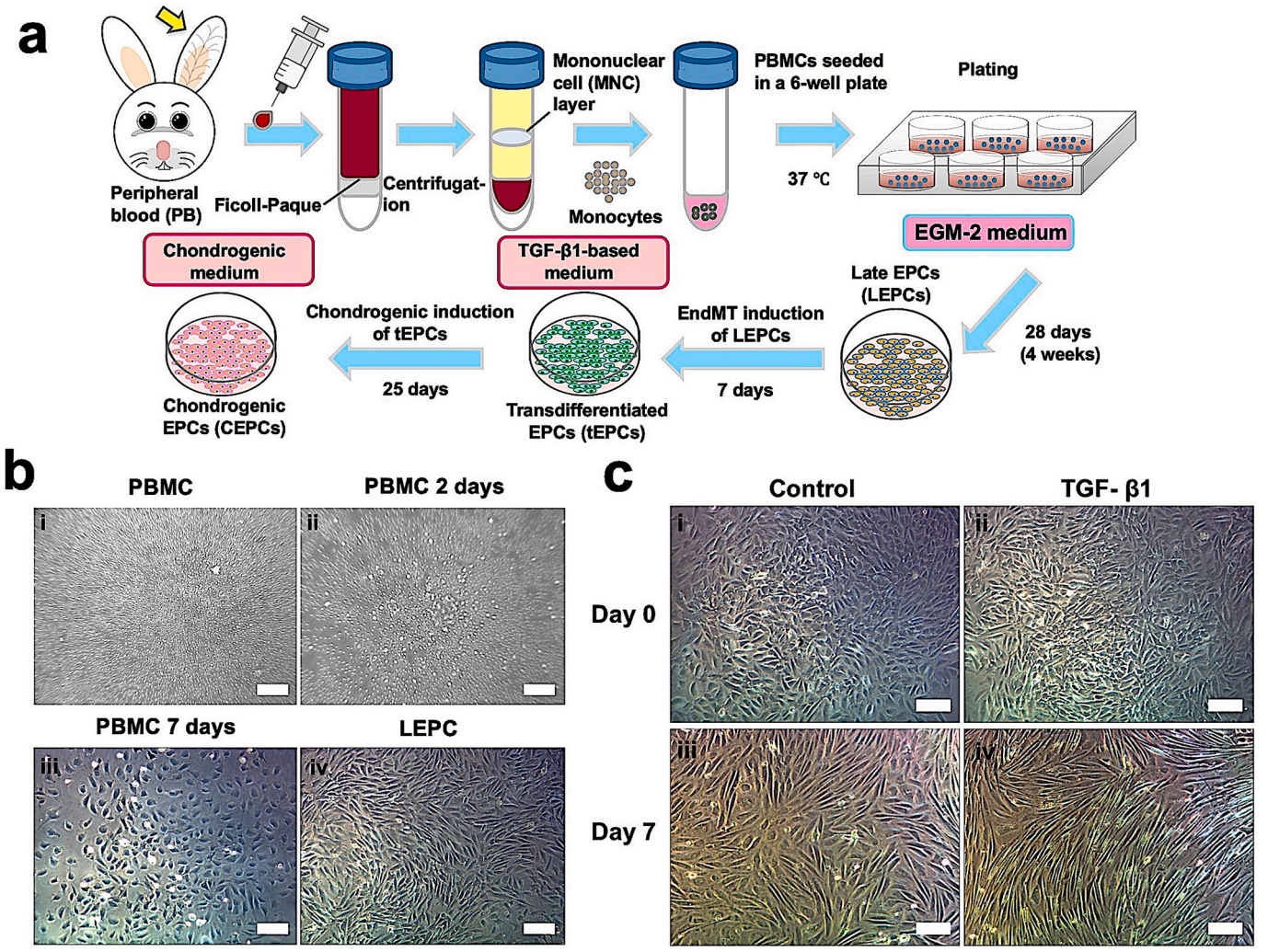

Fig. 1. EPCs derived from peripheral blood differentiate into multiple cell types under TGF-β1 stimulation. (**a**) Schematic of cell culture and differentiation. (**b**) Changes in the cultured EPCs: (**i**) PBMCs immediately after plating, (**ii**) PBMCs 2 days after seeding, (**iii**) PBMCs 7 days after seeding, and (**iv**) exponential growth of LEPCs 14 days after plating (10 × magnification; scale bar: 100 μm). (**c**) Changes in LEPC morphology after TGF-β1 stimulation (days 0 and 7): (**i**, **iii**) LEPCs or (**ii**, **iv**) TGF-β1-stimulated LEPCs (10 × magnification; scale bar: 100 μm). Abbreviations: EGM-2, endothelial growth medium-2; EPCs, endothelial progenitor cells; LEPCs, late EPCs; PBMCs, peripheral blood mononuclear cells; TGF-β1, transforming growth factor-β1.

analyzed the phenotypes of tEPCs after inducing chondrogenesis, osteogenesis, and adipogenesis. The chondrogenic differentiation of tEPCs was induced using a differentiation medium comprising Dulbecco's modified Eagle's medium, 10 % fetal bovine serum (HyClone, Logan, UT, USA), 1 % non-essential amino acids, 100 U/mL penicillin/streptomycin (Gibco BRL), 10 ng/mL TGF-β1, 50 μM L-ascorbate-2-phosphate (Sigma-Aldrich), and 6.25 μg/mL insulin [28]. Expanded cells were subjected to osteogenic and adipogenic differentiation by treating them with osteogenic- and adipogenic-conditioned media (both from ScienCell Research Laboratories, Carlsbad, CA, USA), respectively. Cells undergoing differentiation were treated for 25 days, with the medium replaced every other day. After culture in the aforementioned differentiation media, the cells were analyzed using Alcian Blue, Alizarin Red S, and Oil Red O staining. In addition, the CEPCs were collected for both *in vitro* and *in vivo* experiments (Fig. 1a).

2.3.2. Cell morphology analysis

To examine the effects of TGF-β1 on cell morphology, LEPCs were seeded and cultured at an initial concentration of 1×10^5 cells/mL. After a day of culture, the cells were treated with 10 ng/mL TGF-β1 for 0 and 7 days. Subsequently, cobblestone and spindle-like cells were observed and documented using a phase contrast microscope (BX41; Olympus, Tokyo, Japan).

2.3.3. Colony-forming unit (CFU) efficiency

Stem cell colony formation was assessed as described previously [29]. Briefly, tEPCs from the primary culture were harvested on the sixth day and seeded in six-well plates at a density of 100 cells/well. After 14 days of culture in an incubator (37 °C, 5 % CO_2), the cells were washed with phosphate-buffered saline (PBS), fixed with 75 % ethanol for 15 min, and stained for 30 min with a Crystal Violet Staining Solution (2.3 % certified Crystal Violet, 0.1 % ammonium oxalate, and 20 % ethanol; Sigma-Aldrich). After washing thrice with deionized water, the cell colonies formed in the wells were visualized and counted under a microscope. Colonies comprising over 50 cells were defined as CFUs and counted. The CFU efficiency was calculated using the following formula: CFU efficiency = (counted CFUs/cells originally seeded) × 100.

2.3.4. Flow cytometry analysis of cell surface marker profiles

Flow cytometry analysis was used to examine the expression of cluster of differentiation (CD)44, CD90, and CD105 (MSC markers), CD34 (hematopoietic and endothelial cell marker), and CD45 (leukocyte marker) on the tEPC surface. Following the manufacturer's instructions, tEPCs were harvested from culture dishes upon treatment with 0.25 %

trypsin/ethylenediaminetetraacetic acid in PBS. Next, 1×10^6 tEPCs were suspended in 500 μL of PBS containing 20 μg/mL of fluorescein isothiocyanate (FITC)-conjugated antibodies against CD44 (Novus, Centennial, CO, USA), CD90 (Bioworld, Louis Park, MN, USA), CD105 (Bioss, Woburn, MA, USA), CD34 (Bioss), and CD45 (Bioss). FITC-conjugated non-specific mouse IgG (Bioss) served as an isotype control to exclude non-specific binding. Following a 30-min incubation at 4 °C, the cells were washed three times with PBS and then resuspended in 1 mL of PBS for analysis. Cell samples were analyzed using a BD FACS-Calibur™ instrument (BD Biosciences, Franklin Lakes, NJ, USA).

2.3.5. Immunofluorescence assay

Briefly, tEPCs grown on coverslips were fixed in 4 % paraformaldehyde for 30 min. After blocking with 2 % bovine serum albumin for 1 h, the cells were incubated with primary antibodies, including EC markers (CD31, endothelial nitric oxide synthase [eNOS], VE-cadherin, and vWF; Bioss) or MSC markers (CD44, CD90, and CD105) at 4 °C overnight. Subsequently, the cells were treated with FITC-conjugated secondary IgG (Molecular Probes, Eugene, OR, USA) and 4′,6-diamidino-2-phenylindole (DAPI) (Sigma-Aldrich) at 25 °C in the dark for 1 h. A negative control, lacking treatment with primary antibodies, was included. Cells were visualized and photographed using a scanning confocal microscope (LSM 510 META; Carl Zeiss, Oberkochen, Germany; and TCS SP5; Leica, Wetzlar, Germany).

2.4. In vitro chondrogenic differentiation and signal molecule analysis after TGF-β-induced EndMT in rEPCs

2.4.1. Intracellular sulfated glycosaminoglycan (sGAG)

After the chondrogenic induction of tEPCs for 25 days, we collected CEPCs and detected cartilage-specific extracellular matrix (ECM) formation in induced cells; EPCs without chondrogenic treatment served as a control group. DNA content and sGAG accumulation were quantified via spectrofluorometry using Hoechst 33258 dye and dimethylmethylene blue (DMMB), respectively [30]. Standard curves for the DMMB assay were generated using an aqueous solution of chondroitin sulfate C (Sigma-Aldrich), with concentrations ranging from 0 to 25 μg/μL.

2.4.2. Total collagen synthesis

To quantify collagen synthesis, Sirius Red dye (Direct Red, Sigma-Aldrich) was used to stain total collagen. Briefly, EPCs and CEPCs were collected and lysed using the freeze-thaw method. Cell extracts (50 μL/well) were dispersed in 96-well plates and desiccated in a dry incubator at 37 °C. Each well was washed thrice with 200 μL of distilled H_2O for 1 min/wash. Subsequently, 100 μL of 0.1 % Sirius Red stain (0.05 g of Sirius Red powder per 50 mL picric acid) was added to each well, and the wells were incubated at 25 °C for 1 h. After the unattached stain was removed, the plate was washed five times with 200 μL of 0.1 M HCl. The attached stain was then extracted by agitating the well with 200 μL of 0.1 M NaOH for 5 min. The extracted stain was transferred to a second plate, and the absorbance at a wavelength of 540 nm was determined using a microplate reader (SpectraMax Plus 384; Molecular Devices, Silicon Valley, CA, USA).

2.4.3. Flow cytometry analysis

As described previously, CEPCs were harvested from culture dishes upon treatment with 0.25 % trypsin/ethylenediaminetetraacetic acid in PBS. Subsequently, 1×10^6 CEPCs were suspended in 500 μL of PBS containing 20 μg/mL of FITC-conjugated antibodies targeting CD49c and CD151 (articular chondrocyte surface markers) (Thermo Fisher Scientific). Appropriate isotype control antibodies were used to exclude non-specific binding. After washing, the samples were analyzed using a BD FACSCalibur™ instrument (BD Biosciencces).

2.4.4. Immunofluorescence assay

Briefly, EPCs and CEPCs grown on coverslips were fixed in 4 % paraformaldehyde for 30 min. After blocking with 2 % bovine serum albumin for 1 h, the cells were incubated with primary antibodies against TGF-β type II receptor (TGF-βRII) (Bioworld), signaling molecules (phospho-Smad2 and -Smad3 [P-Smad2 and P-Smad3; Thermo Fisher Scientific], Snail [Bioworld], and phospho-Erk1/2 [P-Erk1/2; Thermo Fisher Scientific]) or chondrocyte transcription factors (sex-determining region Y-box 9 [SOX9; Spring Bioscience, San Francisco, CA, USA]), cartilage-specific ECM (collagen type II [Col II]), and fibrocartilage-specific ECM (collagen type I [Col I]) (Bioss) at 4 °C overnight. Subsequently, the cells were incubated with DAPI (Sigma-Aldrich) and FITC-conjugated secondary IgG (Molecular Probes) at 25 °C in the dark for 1 h. A negative control, not treated with primary antibodies, was included. Cells were visualized and photographed using a scanning confocal microscope (LSM 510 META and TCS SP5).

2.4.5. Immunocytochemistry

After 25 days of culture, CEPCs and EPCs were fixed with 4 % paraformaldehyde and assessed using immunocytochemistry staining. A rabbit-mouse horseradish peroxidase/diaminobenzidine (DAB) polymer detection kit (BioTnA, Kaohsiung, Taiwan) was employed. Primary antibodies against TGF-βRII, P-Smad2, P-Smad3, Snail, P-Erk1/2, SOX9, Col II, and Col I were used at a dilution of 1:100. All staining procedures were performed according to the manufacturer's instructions.

2.4.6. RNA isolation and real-time quantitative polymerase chain reaction (real-time qPCR)

After 25 days of culture, CEPCs and EPCs were harvested for gene expression analysis. TRIzol® reagent (Gibco, Thermo Fisher Scientific) was used to extract total RNA from the cells, according to the manufacturer's instructions. Briefly, 0.5–1 μg of total RNA per 20 μL reaction was reverse-transcribed into cDNA using a SuperScript® First-Strand Synthesis System (Invitrogen, Waltham, MA, USA). Real-time qPCR reactions were performed and monitored using the iQ™ SYBR Green® Supermix and real-time qPCR detection system (both from Bio-Rad Laboratories, Hercules, CA, USA). cDNA samples (2 μL per 25 μL per reaction) were analyzed for both the gene of interest and the reference gene glyceraldehyde-3-phosphate-dehydrogenase (*GAPDH*). The expression level of each target gene was then calculated using the $2^{-\triangle\triangle Ct}$ method. For each gene of interest, four readings were obtained for each experimental sample, and the experiments were repeated at least three times. The primer sequences used are listed in Table S1.

2.4.7. Western blot analysis

Briefly, EPCs and CEPCs were lysed in radioimmunoprecipitation assay buffer (50 mM Tris, 150 mM NaCl, 0.5 % sodium deoxycholate, 1 % nonyl phenoxypolyethoxylethanol, and 0.1 % sodium dodecyl sulfate), and the total protein was extracted and denatured for 5 min at 95 °C. Proteins were separated using 10 % sodium dodecyl sulfate-polyacrylamide gel electrophoresis, transferred onto a polyvinylidene fluoride membrane, and blocked in a 4 % bovine serum albumin blocking buffer. The membrane was then probed with polyclonal antibodies against TGF-βRII, P-Smad2, Smad2 (Bioworld), P-Smad3, Smad3 (Bioworld), and Snail. Furthermore, the membranes were incubated with peroxidase-conjugated anti-rabbit secondary antibodies (Jackson ImmunoResearch, West Grove, PA, USA). In addition, the membranes were reacted with monoclonal antibodies against β-actin (1:5000 dilution, MAB1501; MilliporeSigma, Burlington, MA, USA) and subsequently incubated with peroxidase-conjugated anti-mouse secondary antibodies (Jackson ImmunoResearch). The bands were visualized with Hyperfilm (Amersham Pharmacia, Amersham, Buckinghamshire, UK) using an ECL Plus Kit (Millipore), and the images were analyzed using Mutigel-21 (MGIS-21-C2-1M; TOPBIO Corp., New Taipei, Taiwan).

2.5. Preparation of chitosan-PNIPAAm (CSPN) scaffolds

Porous CSPN scaffolds were manufactured according to the procedure outlined in our previous report [24]. To synthesize the CSPN copolymer, chitosan and NIPAAm monomers were dissolved in 10 mL of a 1 wt% acetic acid solution at 25 °C for 20 min to ensure complete dissolution. The mixture was stirred magnetically and degassed in an oxygen-free nitrogen environment at 4 °C for 30 min. Ammonium persulfate and TEMED were then added as the initiator and accelerator, respectively. The polymerization reaction was performed at 4 °C for 1 day to ensure its completion. Copolymers with a NIPAAm-to-chitosan feeding ratio of 5:1 were prepared. All products were dialyzed against distilled water using a cellulose membrane (molecular weight cut-off = 50 kDa) at 25 °C for 3 days to produce CSPN copolymers, which were subsequently freeze-dried under vacuum conditions.

2.6. Cell culture in CSPN scaffolds

Dry CSPN copolymers were sterilized under ultraviolet irradiation in a laminar flow hood for 1 h and dissolved in sterile PBS at 25 °C to obtain 5 wt% CSPN solutions. The CSPN solutions were then cooled to 4 °C and exposed to ultraviolet irradiation for another 24 h. EPCs and CEPCs were harvested using trypsin (Invitrogen) and mixed with 5 wt% CSPN hydrogel to a cell density of approximately 5×10^6 cells/mL copolymer solution. Before delivering EPC- or CEPC-seeded CSPN scaffolds (EPC-CSPN or CEPC-CSPN, respectively) to animals, the harvested EPCs or CEPCs were labeled with a cell tracker (CM-DiI, Molecular Probes) [31] immediately before seeding onto scaffolds to trace cell fate. After 4 and 12 weeks of implantation, cell proliferation, differentiation, and migration were monitored and observed using a fluorescence microscope (BX51, Olympus) and a Xenogen IVIS® Spectrum System (Caliper Life Sciences, Hopkinton, MA, USA).

2.7. Generation of an in vivo rabbit knee joint OCD model and histopathological examination

The Animal Care and Use Committee of the National Cheng Kung University approved all surgical animal experiments and aseptic procedures (protocol number: 104264). Twenty (40 knees in total) 4–5-month-old New Zealand white male rabbits (each weighing 2–3 kg) were purchased from the Livestock Research Institute, Tainan, Taiwan. The animals were anesthetized with a subcutaneous injection of tiletamine (25 mg/mL) and zolazepam (25 mg/mL; Zoletil® 50; Virbac, Carros, France) combined with a mixture of 2 % isoflurane (Panion & BF Biotech, Taipei, Taiwan) and oxygen, administered through an automatic ventilator for intubation and maintenance. Following anesthesia, both hind legs were sanitized with ethanol, brushed, shaved, disinfected by applying 1 % ethanol-iodine to the target area, and covered with a drape. The knee was accessed through anteromedial parapatellar longitudinal and capsular incisions. The knee joint was then immobilized in a maximally hyper-flexed position, and the patella was laterally dislocated to expose the medial femoral condyles. A full-thickness OCD (3 mm in diameter and 3 mm in depth) was created in the rabbits by drilling the weight-bearing zone of the medial femoral condyle in the knee [32]. Animals subjected to a sham operation (no defect was created in the rabbit knee) were used as the control group ($n = 4$). After OCD surgery, the rabbit knees were immediately injected with CSPN, EPC-CSPN, and CEPC-CSPN ($n = 12$ in each group) into the defect holes (total, 36 knees), and the solutions were gelled using a heat lamp (Video S1). Subsequently, the patellas were repositioned in their correct positions, and the incisions were closed. The joint capsule was sutured using 3–0 absorbable Vicryl sutures (Ethicon, Bridgewater, NJ, USA), and subcutaneous tissues and skin wounds were repaired using 3–0 nylon sutures. After the operation, the control, CSPN, EPC-CSPN, and CEPC-CSPN groups were allowed free activity in their cages. After 4 or 12 weeks, the rabbits were euthanized by administering an overdose of the anesthetic agent and intravenous injection of potassium chloride. Repaired osteochondral tissues were harvested for further examination.

Supplementary video related to this article can be found at https://doi.org/10.1016/j.mtbio.2024.101174

2.8. Macroscopic evaluations

After postoperative euthanasia at 4 and 12 weeks (CSPN, EPC-CSPN, and CEPC-CSPN groups: 6 knees each at each time-point; control group: 4 knees), two researchers blindly determined the macroscopic scores for the reparative tissues using our previously established scoring system [33], which considers coverage, tissue color, and surface condition. The maximum total score was 12 points (Table S2).

2.9. Histological and immunohistochemical processing

Histological sections were prepared by the Department of Pathology of the Chi-Mei Medical Center (Tainan, Taiwan) using standard procedures, including 10 % formalin fixation, dehydration in gradient ethanol solutions, decalcification, infiltration, and paraffin embedding. Sections were prepared (4-μm thick) and stained with hematoxylin and eosin to assess cell morphology and regenerative tissue matrix distribution, Masson's trichrome to determine the collagen content, and Safranin O/Fast Green Stain to analyze the sGAG content. Microscopic examination was performed using a microscope (BX51, Olympus), and sections were imaged using a digital CCD (DP70, Olympus). Furthermore, to determine the contents of Col II (hyaline cartilage) and Col I (fibrocartilage) in the regenerated tissues, the sections were subjected to immunohistochemical analysis using anti-Col II and I antibodies (1:100 dilution), and the rabbit/mouse horseradish peroxidase/DAB polymer detection kit, according to the manufacturer's standard protocols. Quantitative analysis of Safranin O staining and Col II and I staining were performed using ImageJ 1.50i software (National Institutes of Health, Bethesda, MD, USA).

2.10. Micro-computed tomography (micro-CT) evaluations

To individually perform qualitative and quantitative measurements of bone regeneration within the defects, the medial femoral condyles of the CSPN, EPC-CSPN, and CEPC-CSPN groups were scanned using a microtomography 1076 scanner (Skyscan 1076; Bruker Corp., Billerica, MA, USA). The CSPN, EPC-CSPN, and CEPC-CSPN groups (12 knees in each group) were compared at 4 and 12 weeks post-operation. The formalin-fixed ends of the rabbit femurs were loaded onto a sample holder, aligning the femur axis perpendicular to the scanning plane. Considering the X-ray source parameters or assessing the mineralized tissue, the voltage was set to 50 kV and the current was set to 160 μA [33]. The samples were scanned through a 360° rotation angle with a rotation interval of 1° and a pixel size with 18 μm resolution. The Skyscan software package was used to analyze the image data and visualize the new bone matrix. Within the CT dataset, a cylindrical region of interest (diameter, 3 mm), encompassing the repaired site and corresponding to the original defect region, was selected for analysis. Bone volume and diameter were measured as bone volume per tissue volume (BV/TV) and trabecular thickness (Tb.Th), respectively.

2.11. Statistical analysis

All data are presented as the mean ± standard error of the mean. All statistical analyses were performed using SPSS Statistics for Windows, version 17.0 (IBM Corp., Chicago, IL, USA). One-way analysis of variance was applied, and multiple comparisons were performed using the Scheffe method. Statistical significance was set at $P < 0.05$.

3. Results

3.1. EPCs exhibit LEPC characteristics

Initially, the seeded cells had a round morphology (Fig. 1b–i). After 2 days, attached cells formed clusters (Fig. 1b–ii) with an elongated, spindle-shaped appearance similar to that of EPCs [34]. These cells, termed early EPCs (Fig. 1b–iii), did not replicate *in vitro* and gradually disappeared after 4 weeks. Distinct LEPCs with varying morphologies emerged after 2 weeks, exhibiting a smoother cytoplasmic outline, robust attachment to the plate, and a cobblestone appearance similar to cultured endothelial cells (Fig. 1b–iv). The LEPCs rapidly replicated from several cells to a colony, establishing a monolayer with almost full confluence, and underwent multiple population doublings without senescence.

3.2. TGF-β1-induced LEPCs acquire stem cell-like properties

EPCs exhibited fibroblast-like morphology 7 days after TGF-β1-induced EndMT, suggesting that tEPCs may possess MSC-like properties (Fig. 1c). We then examined the surface marker profile of tEPCs to confirm their MSC identity (passage 3). Flow cytometry showed that the tEPCs expressed CD44, CD90, and CD105 but not CD34 and CD45 (Fig. 2a). Immunofluorescence staining revealed that tEPCs expressed CD44, CD90, and CD105 but not CD31, eNOS, VE-cadherin, and vWF (Fig. 2b). The CFU assay revealed that the tEPCs contained a subpopulation of cells capable of generating new fibroblast colonies from single cells (Fig. 2c). tEPCs established multiple large colonies compared to EPCs, which exhibited fewer and smaller colonies. The CFU efficiency varied between the groups ($P = 0.000001$; Fig. 2d). tEPCs exhibited higher CFU efficiency than EPCs (9.83 % *vs.* 0.81 %, respectively), confirming the MSC-like properties of tEPCs.

To confirm the multilineage differentiation potential of culture-expanded tEPCs, tEPCs were subjected to chondrogenic, osteogenic, and adipogenic differentiation. After chondrogenic induction, tEPCs formed Alcian Blue-positive cartilaginous nodules (Fig. 2e–i). Osteogenic induction resulted in the positive Alizarin Red S staining of calcium compounds in the mineralized matrix of tEPCs (Fig. 2e–ii). Upon adipogenic induction, tEPCs developed Oil Red O-positive lipid droplets (Fig. 2e–iii), confirming the multilineage differentiation potential of induced tEPCs.

3.3. tEPCs redifferentiate into CEPCs under TGF-β1-induced chondrogenic stimuli

To investigate the effect of EndMT induction on the chondrogenic

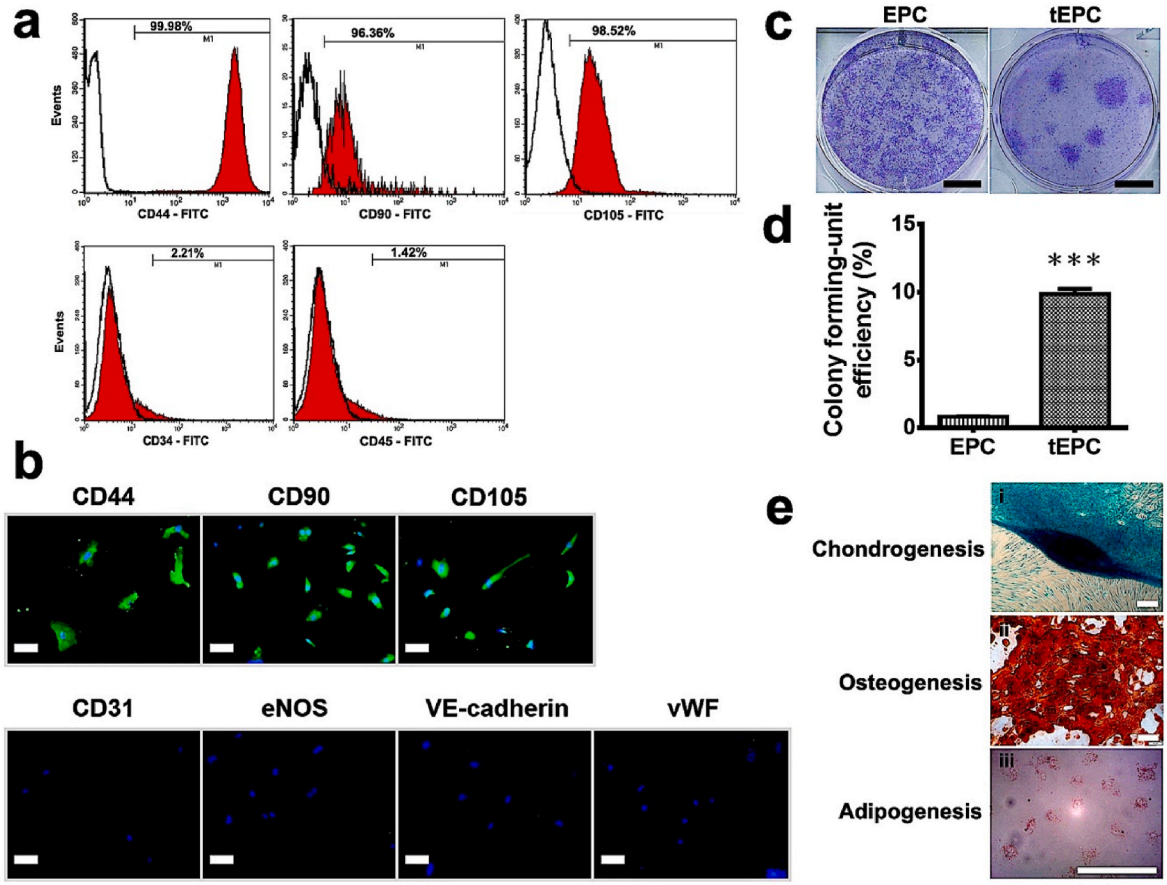

Fig. 2. EndMT-derived tEPCs acquire an MSC-like phenotype. (**a**) Flow cytometry analysis of CD44, CD90, CD105 (mesenchymal stem cell markers), CD34 (hematopoietic and endothelial cell marker), and CD45 (leukocyte marker) expression in tEPCs. The empty areas show isotype control staining. The red-filled areas represent the expression of specific markers. (**b**) Representative immunofluorescence images of tEPC surface markers. tEPCs stain positive for MSC markers (CD44, CD90, and CD105) and negative for endothelial cell markers (CD31, eNOS, VE-cadherin, and vWF) (20 × magnification; scale bar: 50 μm). (**c**, **d**) CFU efficiency of EPCs and tEPCs, assessing self-renewal through the rate of colony formation in CFU assays. (**c**) Representative colonies of EPCs and tEPCs in 6-well plates (scale bar: 5 mm). (**d**) Columns illustrate the CFU efficiency. Values are reported as the mean ± standard deviation (SD) of six replicates. ***$P < 0.001$. (**e**) Multilineage differentiation potential of tEPCs induced to differentiate into (**i**) chondrogenic (10 × magnification; scale bar: 100 μm), (**ii**) osteogenic (10 × magnification; scale bar: 100 μm), or (**iii**) adipogenic (40 × magnification; scale bar: 10 μm) lineages. Abbreviations: CD, cluster of differentiation; CFU, colony-forming unit; EndMT, endothelial-to-mesenchymal transition; eNOS, endothelial nitric oxide synthase; EPCs, endothelial progenitor cells; MSC, mesenchymal stem cell; tEPC, trans-differentiated EPCs; VE-cadherin, vascular endothelial cadherin; vWF, von Willebrand factor.

potential of EPCs *in vitro*, tEPCs were cultured in a TGF-β1-containing chondrogenic medium for 25 days to induce chondrogenic differentiation. The EPC and CEPC groups were then compared in terms of cell aggregation, chondrogenic gene expression, chondrocyte surface marker expression, cartilaginous matrix synthesis, sGAG deposition, and total collagen synthesis (Fig. 3). Cell aggregation was observed 25 days after the tEPCs were cultured in a chondrogenic medium, whereas no aggregation was observed in the EPC control group (Fig. 3a-i, 3a-ii).

Alcian Blue staining and the DMMB assay were used to confirm the deposition of sGAG in the EPC and CEPC groups. Alcian Blue staining revealed more intense sGAG deposition in tEPCs cultured in a chondrogenic medium for 25 days than in the EPC control group (Fig. 3a-iii, 3a-iv). The DMMB assay showed that the average rate of sGAG synthesis was higher in the CEPC group than in the EPC control group (Fig. 3b). Similarly, after 25 days, the CEPC group produced higher levels of total intracellular collagen than the EPC control group (Fig. 3c).

Real-time qPCR was used to confirm the expression of chondrogenic genes in the CEPC and EPC control groups. After 25 days, the expression of *Col I* ($P = 0.01$), *Col II* ($P = 0.006$), aggrecan (*ACAN*; $P = 0.0004$), and *SOX9* ($P = 0.03$) was significantly higher in the CEPC group than in the EPC control group (Fig. 3d). Flow cytometry revealed that up to 99 % of CEPCs stained positive for the articular chondrocyte surface markers CD49c and CD151 (Fig. 3e), suggesting that EndMT enhances EPC chondrogenesis *in vitro*. After chondrogenic induction, tEPCs exhibited enhanced cell aggregation, elevated chondrogenic gene expression, increased cartilaginous matrix synthesis, and chondrocyte-like surface marker expression.

3.4. TGF-β signaling is involved in EPC transdifferentiation and redifferentiation, as well as chondrogenic matrix protein synthesis

TGF-βRII, P-Smad2/3, P-Erk1/2, Snail, SOX9, and Col I/II levels were then compared using immunofluorescence and immunocytochemical staining. CEPCs exhibited stronger staining for all proteins than EPCs (Fig. 4a and b). Furthermore, the levels of TGF-βRII, P-Smad2/3, Smad2/3, and Snail were compared using western blotting. After 25 days of culture, CEPCs displayed increased levels of TGF-βRII, P-Smad2/3, Smad2/3, and Snail compared with EPCs (Fig. 4c and d). These results indicated that the levels of TGF-βRII, P-Smad2/3, Smad2/3, P-Erk1/2, Snail, SOX9, and Col II were enhanced in CEPCs, along with EndMT induction and chondrogenesis in EPCs.

3.5. In vivo evaluation of the regenerative potential of cell-scaffold constructs in OCDs using rabbit models

3.5.1. Cell-seeded scaffolds implanted into OCDs stimulate cartilage repair

To examine OCD repair induced by EPC/CEPC-CSPN scaffolds, full-thickness OCDs were generated in the weight-bearing area of rabbit

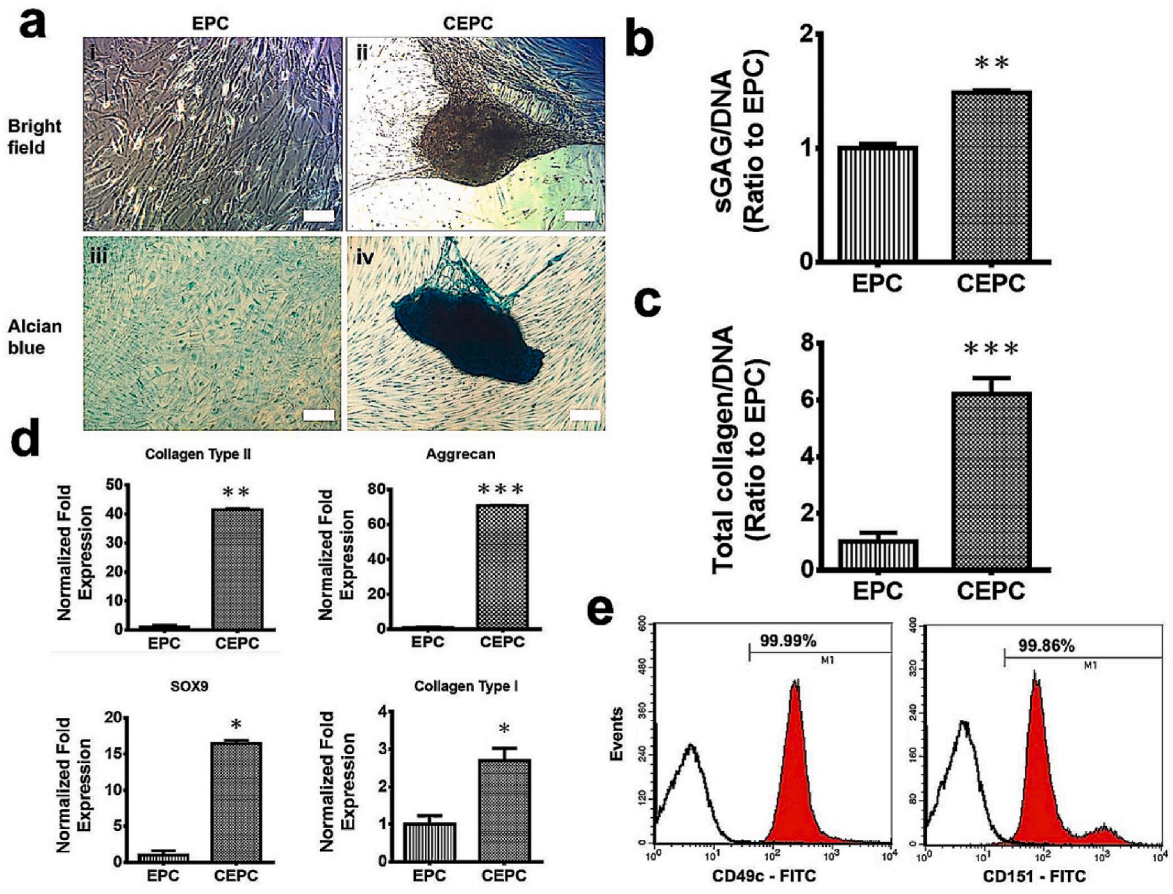

Fig. 3. TGF-β1 induces tEPC activation and differentiation into chondrocyte-like cells that secrete cartilage-specific proteins. (**a**) Morphology of tEPCs after chondrogenic induction for 25 days: (**i**, **iii**) EPCs (control group) and (**ii**, **iv**) tEPCs after chondrogenic induction (CEPC group). EPCs and CEPCs were stained with Alcian Blue to assess the sGAG content (10 × magnification; scale bar: 100 μm). (**b**) sGAG synthesis in EPCs and CEPCs. (**c**) Intracellular collagen synthesis by EPCs and CEPCs. (**d**) mRNA expression of chondrogenic genes (*ACAN*/*SOX9*/*Col II*) and the fibrocartilage marker, *Col I*, in EPCs and CEPCs (day 25). Expression levels are expressed relative to those of the control group (defined as 1). Values are reported as the mean ± standard deviation (SD) of four replicates. $^{*}P < 0.05$, $^{**}P < 0.01$, and $^{***}P < 0.001$. (**e**) Flow cytometric confirmation of CD49c and CD151 expression on the surface of CEPCs, with up to 99 % of the CEPC population staining positive for CD49c (red area) and CD151 (red area) compared with isotype control CEPCs (white area). Abbreviations: *ACAN*, aggrecan; CD, cluster of differentiation; CEPCs, chondrogenic EPCs; *Col I*, collagen type I; *Col II*, collagen type II; EPCs, endothelial progenitor cells; sGAG, sulfated glycosaminoglycan; *SOX9*, sex-determining region Y-box 9; tEPCs, transdifferentiated EPCs; TGF-β1, transforming growth factor-β1.

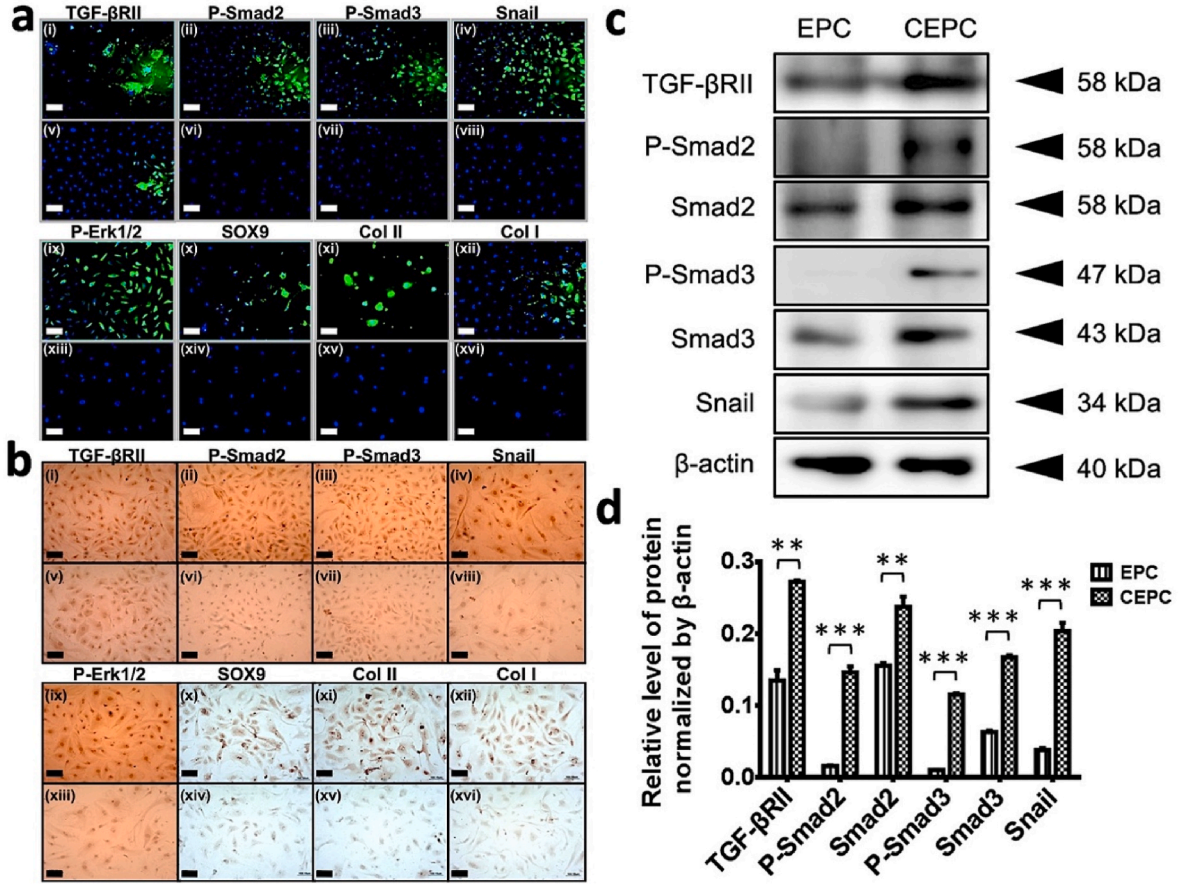

Fig. 4. TGF-β signaling drives EndMT progression and regulates the chondrogenic differentiation of EPCs. CEPCs generated from EPCs were induced to undergo EndMT (via treatment with TGF-β1 for 7 days; tEPCs) and chondrogenic differentiation (for another 25 days). (**a**) Immunofluorescence (20 × magnification; scale bar: 50 μm) and (**b**) immunocytochemical (10 × magnification; scale bar: 10 μm) staining of (**v–viii**, **xiii–xvi**) EPCs and (**i–iv**, **ix–xii**) CEPCs *in vitro*. CEPCs stain positive for TGF-βRII, P-Smad2/3, Snail, P-Erk1/2, SOX9, and Col I/II (green and brown). DAPI counterstaining (blue). (**c**) Protein expression of EndMT signaling molecules (TGF-βRII, P-Smad2/3, Smad2/3, and Snail) in EPCs and CEPCs (day 25). (**d**) Protein expression of TGF-βRII, P-Smad2/3, Smad2/3, and Snail in EPCs and CEPCs after being normalized to β-actin (day 25). Values are reported as the mean ± standard deviation (SD) of three replicates. $^{**}P < 0.01$ and $^{***}P < 0.001$. Abbreviations: CEPCs, chondrogenic EPCs; Col I, collagen type I; Col II, collagen type II; DAPI, 4′,6-diamidino-2-phenylindole; ECM, extracellular matrix; EndMT, endothelial-to-mesenchymal transition; EPCs, endothelial progenitor cells; Erk, extracellular signal-regulated kinase; P, phosphorylated; SOX9, sex-determining region Y-box 9; TGF-βRII, TGF-β type II receptor; tEPCs, transdifferentiated EPCs; TGF-β, transforming growth factor-β.

medial femoral condyles. Fig. 5 illustrates the establishment of the OCD model and the surgical procedure performed in the *in vivo* study.

3.5.2. *CEPC-CSPN scaffolds improve the regenerative capacity of cartilage*

No rabbit experienced joint swelling, infection, limited range of motion, or osteophyte formation at 4 and 12 weeks post-surgery. The knees showed no visible residue of material yet exhibited some regeneration. At week 4, the CSPN group displayed yellow-red repair tissue adjacent to OCD. The OCD was concave, and the margin was visible. In contrast, the OCDs in the EPC-CSPN and CEPC-CSPN groups were less visible, with a white-yellow appearance. The new tissue had a rough articular surface, and the OCD boundary was still visible. At week 12, the OCDs in the EPC-CSPN and CEPC-CSPN groups were nearly filled with repair tissue. The regeneration sites in the CEPC-CSPN group contained abundant repair tissue with a smooth articular surface and predominantly transparent, new hyaline-like tissue integrated with adjacent tissue. However, in the CSPN group, the OCDs were filled with yellow-red regenerative tissue with an irregular articular surface and a clear boundary. The EPC-CSPN group exhibited OCDs covered with new opaque tissue, with a low degree of cartilage-like transparent tissue formation and repair clefts that are still visible (Fig. 6a). At week 4, the CEPC-CSPN group had a higher macroscopic score (8.6 ± 0.33) than the CSPN (5.0 ± 0.57; $P = 0.004$) and EPC-CSPN (7.3 ± 0.33; $P = 0.02$) groups; there was a significant difference between the CSPN and EPC-CSPN groups ($P = 0.01$). At week 12, the CEPC-CSPN group had a higher score (10.7 ± 0.33) than the CSPN (7.3 ± 0.33; $P = 0.001$) and EPC-CSPN (9.0 ± 0.57; $P = 0.04$) groups; there was a significant difference between the CSPN and EPC-CSPN groups ($P = 0.04$; Fig. 6b).

3.5.3. *CEPCs are present in regenerating cartilage and bone*

To monitor the implanted EPCs and CEPCs *in vivo*, the encapsulated cells were labeled with the cell tracker CM-DiI. Fluorescent cells in OCD were observed after 4 (Fig. 6c-i, 6c-ii) and 12 weeks (Fig. 6c–iii, 6c-iv), confirming successful EPC and CEPC implantation. Following sectioning, red fluorescence was observed in the regenerated tissue in the OCDs, as assessed via fluorescence microscopy (Fig. 6d), suggesting that cell migration occurs from the subchondral bone (Fig. 6d-i, 6d-ii) to the cartilage (Fig. 6d-iii, 6d-iv) during regeneration. In the CEPC-CSPN group, cells were observed in the cartilage 4 weeks after implantation (Fig. 6d-ii).

3.5.4. *CEPC-CSPN scaffolds enhance cartilage repair through the chondrogenic potential of CEPCs*

At week 4, the repaired joints in the CEPC-CSPN group displayed extensive tissue coverage, with abundant chondroblasts and limited fibroblast migration to the top and middle of the repaired chondral

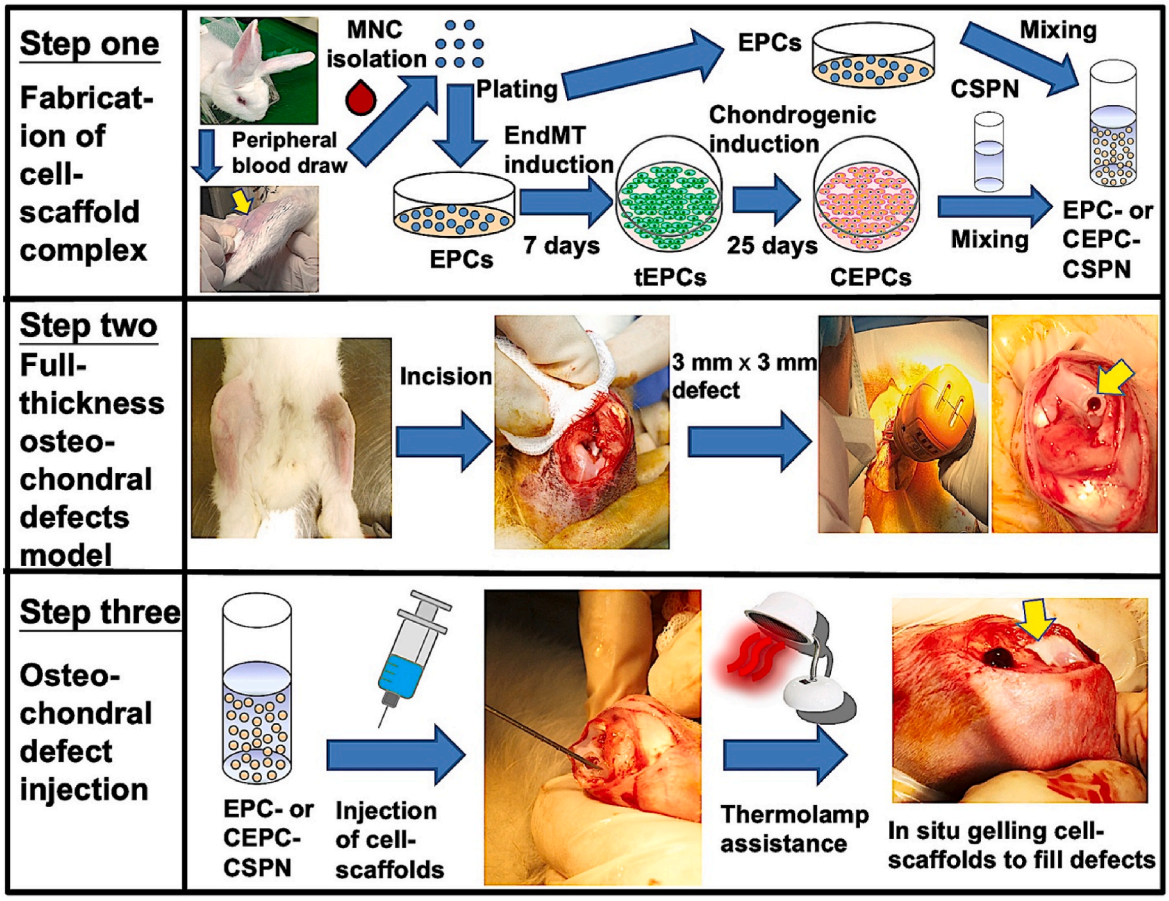

Fig. 5. Schematic illustration of the surgical procedure for implantation of a cellular scaffold in a full-thickness osteochondral injury within the weight-bearing area of the medial femoral condyle of a rabbit. MNC, mononuclear cell; EPCs, endothelial progenitor cells; tEPCs, transdifferentiated EPCs; CEPCs, chondrogenic EPCs; EndMT, endothelial-to-mesenchymal transition; CSPN, chitosan-graft-poly (N-isopropylacrylamide); EPC-CSPN, CSPN scaffold containing EPCs; CEPC-CSPN, CSPN scaffold containing CEPCs.

layer. However, the repaired joints in the EPC-CSPN group were covered with disorganized fibrous tissue and partial hyaline-like cartilage tissue with fibroblast-like cells and immature chondrocytes. Meanwhile, the joints in the CSPN group had a disrupted and depressed surface, and the OCDs were filled with fibrous or immature repair tissue. The CEPC-CSPN group exhibited immature tissue at the top of the chondral layer of the regenerated tissue. The EPC-CSPN and CEPC-CSPN groups had chondroblasts and synovial-like cells that were overly fibrous. Moreover, the CEPC-CSPN group had more osteoid matrix and compact bone in the repaired subchondral bone plate than the CSPN and EPC-CSPN groups. Compared with the CSPN group, the EPC-CSPN group had more newly formed bone tissue, which had penetrated the center of the scaffold and was visible as compact bone without trabecular bone. The junction between the repaired and surrounding native tissue could be easily distinguished (Fig. 7a).

Regarding collagen and sGAG synthesis, the CEPC-CSPN group exhibited stronger Masson's trichrome (Fig. 7b) and Safranin O/Fast Green (Fig. 7c) staining in the neocartilage tissue at the repair site. The EPC-CSPN group had modest collagen and sGAG contents in the new and adjacent cartilage. In contrast, only slight collagen and sGAG staining were observed at the repair site in the CSPN group. Regarding the synthesis of cartilage-specific matrix, the CEPC-CSPN group expressed high levels of Col II (Fig. 7d) and had low levels of Col I (Fig. 7e) both in the newly regenerated tissue and adjacent cartilage. In contrast, the CSPN and EPC-CSPN groups had high levels of Col I and low levels of Col II.

At week 12, the CEPC-CSPN group had a smooth articular surface with nearly normal hyaline cartilaginous structures (Fig. 7a), good chondrocyte alignment, abundant collagen (Fig. 7b), high sGAG content (Fig. 7c), and a reconstructed bone structure. The newly regenerated tissue integrated well with the surrounding cartilage and bone, showing uniformly thick neocartilage. The chondrocytes had a typical lacuna structure with elongated morphology and were perpendicular to the surface, consistent with hyaline-like regenerated tissue. The CEPC-CSPN group had a more functionally mature trabecular bone embedded with osteocytes and a more osteoid matrix in the subchondral bone. In contrast, the EPC-CSPN group had fibrocartilaginous tissue with moderate sGAG content; chondroblasts and small dispersed chondrocytes were observed in the newly formed chondral layer. The collagen fibers were thinner and more disorganized in the EPC-CSPN group than those in the CEPC-CSPN group. However, good integration was observed between the repair and the host tissue. The repair site in the subchondral bone of the EPC-CSPN group displayed more osteoid matrix, compact bone formation, and osteoblasts than that in the CSPN group. The tidemark was restored in both the EPC-CSPN and CEPC-CSPN groups. In contrast, the CSPN group had fibrous tissue mixed with irregular bone islands in the chondral layer and low collagen and sGAG content in the OCD. The cell arrangement was poor, with cracks at the integration site. Based on the immunostaining results, the repair tissue matrix in the CEPC-CSPN group displayed enhanced Col II (Fig. 7d) and reduced Col I (Fig. 7e) expression compared with that in the CSPN and EPC-CSPN groups. The EPC-CSPN group exhibited partial original hyaline cartilage structures with higher levels of Col II and lower levels of Col I than the CSPN group.

Based on the histological assessment, the EPC-CSPN and CEPC-CSPN groups had increased sGAG deposition at 4 and 12 weeks compared to the CSPN group. Safranin O/Fast Green staining revealed that CEPC-

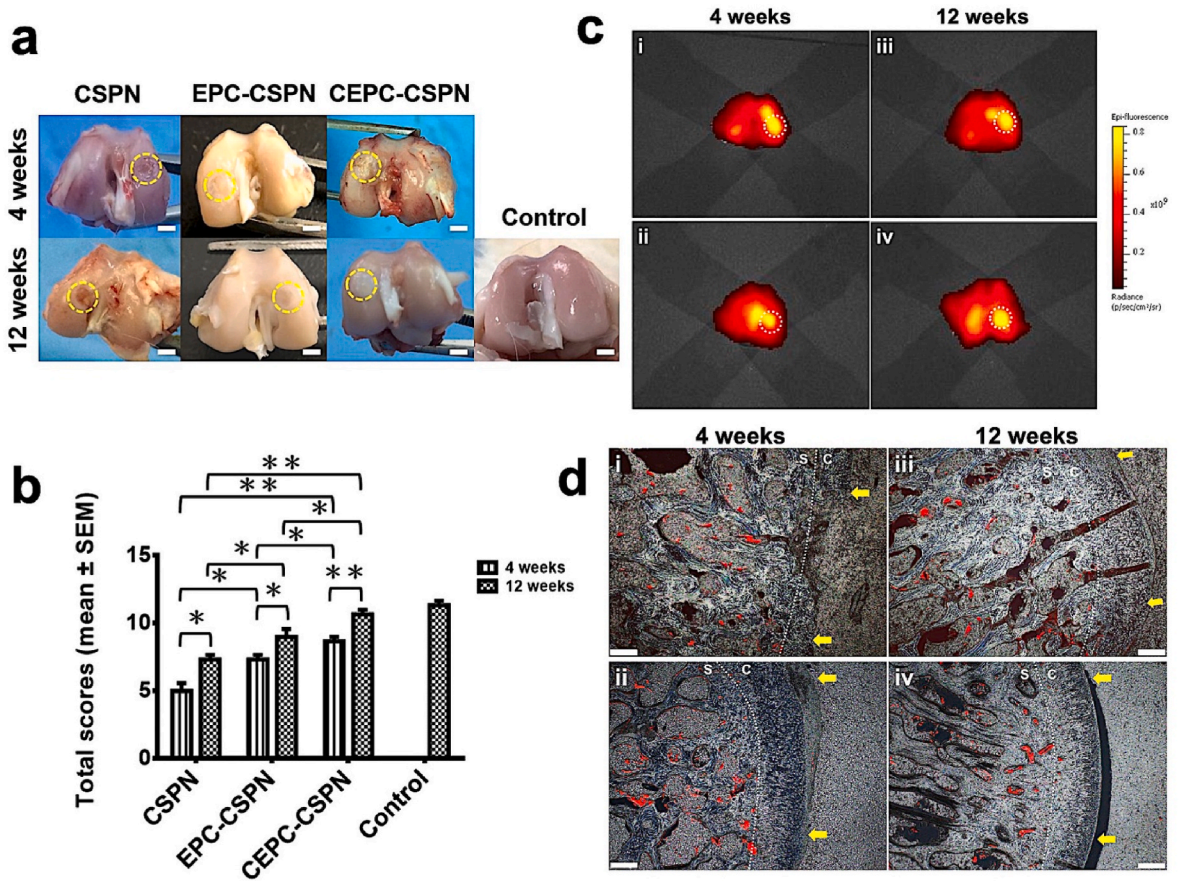

Fig. 6. Damaged cartilage can be effectively repaired by applying CEPC-based scaffolds to the affected area. (**a**) Representative photographs show the gross appearances of the scaffolds or cell scaffolds in cartilage defects at 4 and 12 weeks post-operation. Yellow circles represent the cartilage defect sites. Scale bar: 2 mm. (**b**) Quantitative gross appearance scores calculated at 4 and 12 weeks post-surgery. The reported values are the average of $n = 6 \pm$ standard deviation. $^{*}P < 0.05$ and $^{**}P < 0.01$. (**c**) Representative *in vitro* fluorescence imaging of DiI-labeled cells in the EPC-CSPN and CEPC-CSPN constructs in the cartilage defects at weeks 4 and 12 post-operation. (**i**) and (**iii**): Fluorescence images of EPCs in the EPC-CSPN constructs at the defect sites. (**ii**) and (**iv**): Fluorescence images of CEPCs in the CEPC-CSPN constructs at the defect sites. White circles represent cartilage defect sites, whereas the yellow areas represent DiI-labeled cells. (**d**) Fluorescence images obtained using fluorescence microscopy after paraffin sectioning. The EPC-CSPN and CEPC-CSPN constructs were implanted for 4 and 12 weeks. (**i**) and (**iii**): Fluorescence images of EPCs in the EPC-CSPN constructs at the defect sites. (**ii**) and (**iv**): Fluorescence images of CEPCs in the CEPC-CSPN constructs at the defect sites. The red areas represent DiI-labeled cells. Magnification: 4 × ; scale bar: 200 μm. Yellow arrows indicate the borders of defects. Abbreviations: C, cartilage layer; S, subchondral bone layer; EPCs, endothelial progenitor cells; CEPCs, chondrogenic EPCs; CSPN, chitosan-graft-poly (N-isopropylacrylamide); EPC-CSPN, CSPN scaffold containing EPCs; CEPC-CSPN, CSPN scaffold containing CEPCs.

CSPN scaffolds had the highest sGAG deposition (Fig. 7f). At weeks 4 and 12, the EPC-CSPN and CEPC-CSPN groups had higher Col II (Fig. 7g) and lower Col I (Fig. 7h) staining intensities than the CSPN group. Similarly, CEPC-CSPN scaffolds had the highest Col II and lowest Col I deposition, suggesting that they promote hyaline cartilage regeneration for cartilage repair.

3.5.5. *CEPC-CSPN scaffolds promote subchondral bone regeneration*

At week 4, the newly synthesized mineralized matrix regenerated from the outer surface of the OCD in the three groups (Fig. 8a). However, the CEPC-CSPN group had a higher volume of regenerated bone than the CSPN and EPC-CSPN groups. Based on the sagittal view of the central repair site, the growth pattern of mineralized bone was outer-to-middle. Differences in the BV/TV and Tb.Th values were observed between the EPC-CSPN and CEPC-CSPN groups (both $P < 0.01$). The EPC-CSPN and CEPC-CSPN groups had higher BV/TV values than the CSPN group ($P < 0.01$). The CSPN and EPC-CSPN groups had lower BV/TV values than the control group ($P < 0.01$; Fig. 8b). There was no significant difference in the Tb.Th values between the CSPN and EPC-CSPN groups and the control group (Fig. 8c). The control group had higher BV/TV and Tb.Th values than the CEPC-CSPN group (both $P < 0.01$).

At week 12, the repair site of the EPC-CSPN group had more newly mineralized tissue adjacent to the center of the OCD than the repair sites of the CSPN and CEPC-CSPN groups (Fig. 8a). Complete bridging of the OCD by mineralized bone was observed in the EPC-CSPN and CEPC-CSPN groups. The regenerated tissue had a higher BV/TV in the EPC-CSPN group than in the CSPN and CEPC-CSPN groups (both $P < 0.01$; Fig. 8b). The EPC-CSPN group had a higher BV/TV than the control group ($P < 0.01$). There were no significant differences in BV/TV between the CEPC-CSPN and control groups. The three groups showed significantly different BV/TV values between weeks 4 and 12 (all $P < 0.01$). The EPC-CSPN group had a higher Tb.Th value than the control group ($P < 0.01$; Fig. 8c), while there was no significant difference in Tb.Th between the CEPC-CSPN and the control groups. The EPC-CSPN ($P < 0.01$) and CEPC-CSPN ($P < 0.05$) groups showed significantly different Tb.Th values between weeks 4 and 12.

4. Discussion

Current treatments for cartilage-related injuries have limitations. Peripheral blood-derived EPCs offer an alternative that avoids invasive procedures, minimizes postoperative discomfort, and is relatively straightforward, with no donor site morbidity. EPC transplantation has been explored to treat articular cartilage defects. In addition, a few

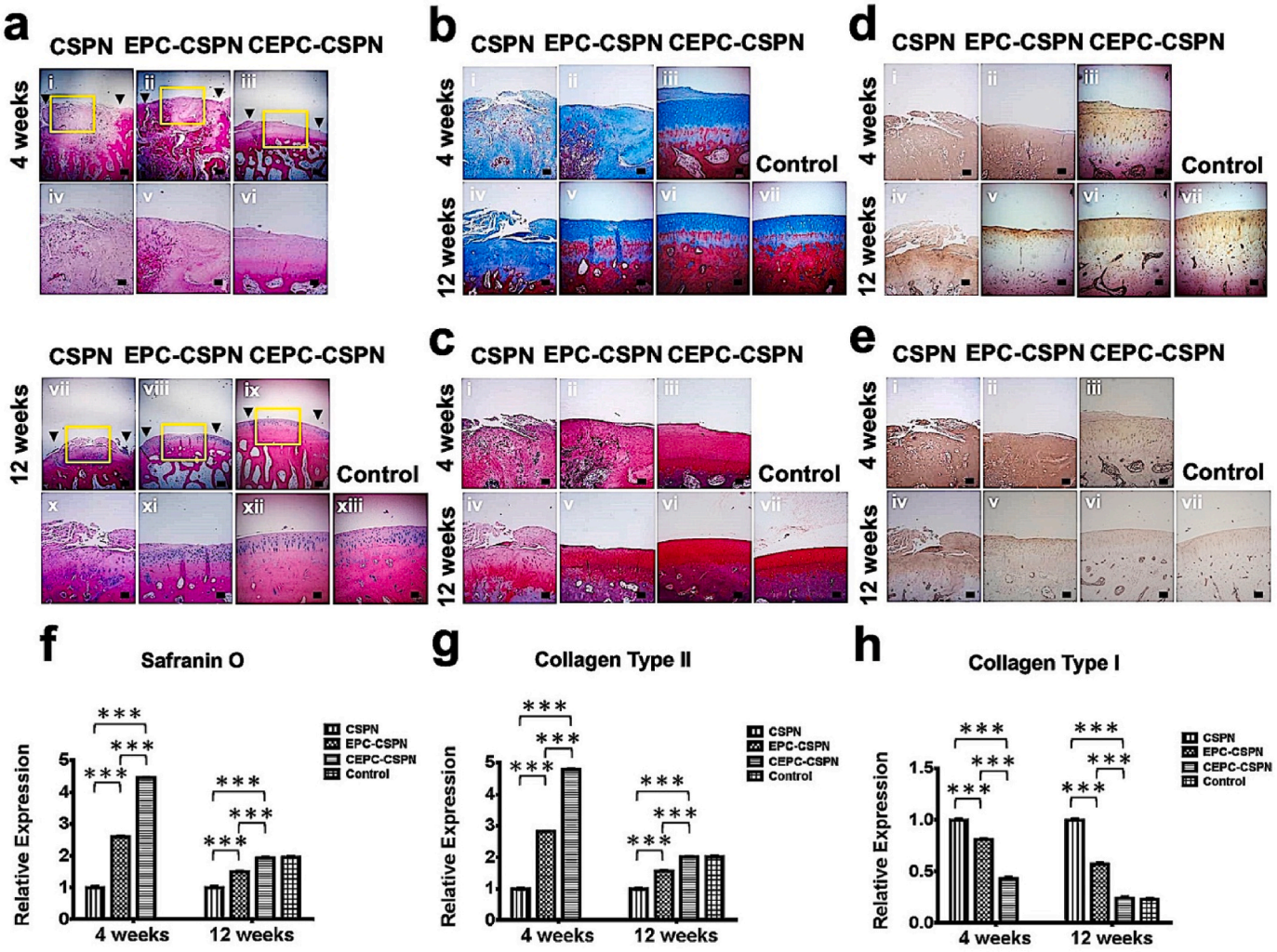

Fig. 7. CSPN scaffolds require CEPCs to induce hyaline cartilage regeneration. Representative sections of defects filled with CSPN, EPC-CSPN, or CEPC-CSPN were stained using histochemical methods, including H&E (**a**), Masson's trichrome (**b**), and Safranin O/Fast Green staining (**c**). Sections were also subjected to immunostaining of collagen types II (**d**) and I (**e**). The area enclosed by the yellow box is shown enlarged underneath the main figure (**a-iv-vi** and **a-x-xii**). Black arrows indicate the borders of the defects. The original magnifications of the H&E images were 4 × (**a-i–iii** and **a-vii–ix**; scale bar: 200 μm) and 10 × (**a-iv–vi** and **a-x–xiii**; scale bar: 100 μm). The original magnifications of the Masson's trichrome (**b-i–vii**) and Safranin O/Fast Green (**c-i–vii**) staining images, immunostaining images for collagen types II (**d-i–vii**) and I (**e-i–vii**) were 10 × (Scale bar: 100 μm). Quantitative analysis of Safranin O (**f**) and collagen types II (**g**) and I (**h**) staining intensities, normalized relative to those in the CSPN group, which were defined as 1. The reported values are the average of $n = 6 \pm$ standard deviation. $^{***}P < 0.001$. Abbreviations: H&E, hematoxylin and eosin; EPCs, endothelial progenitor cells; CEPCs, chondrogenic EPCs; CSPN, chitosan-graft-poly (N-isopropylacrylamide); EPC-CSPN, CSPN scaffold containing EPCs; CEPC-CSPN, CSPN scaffold containing CEPCs.

studies [10,11] have shown that endothelial cells can transdifferentiate into mature chondrocytes and osteocytes through TGF-β-induced EndMT. Based on these findings, EPCs have emerged as a potential source of MSCs. Therefore, in this study, we employed TGF-β1 to induce EndMT in EPCs and evaluate the stem cell-like properties and chondrogenic potential of the resultant cells *in vitro*.

In the current study, tEPCs exhibited MSC-like properties. Our findings suggest that peripheral blood-derived EPCs encompass not only endothelial precursors but also multipotent precursors or a group of monopotent precursors for several distinct lineages. Therefore, EPC-derived MSCs appear to be multipotent rather than a mixture of committed progenitor cells.

Previous studies [10,35] have focused on the role of EndMT in disease and disease treatment. However, EndMT can also be used to obtain multipotent MSCs from endothelial cells that can be easily redifferentiated into various different cell types [9]. One well-studied mediator of EndMT is the TGF-β family of growth factors [12,36], which mediate signals through Smad-dependent and -independent pathways. In this study, EPCs differentiated into stem-like cells through TGF-β1-induced EndMT (Figs. S1 and S2), which involves the same molecules as the TGF-β/Smad pathway, consistent with previous studies [18,37]. TGF-β1 also induced the EndMT of EPCs through the non-canonical mitogen-activated protein kinase/Erk pathway (Figs. S1 and S2). Accordingly, we demonstrated the involvement of canonical and non-canonical TGF-β pathways in the redifferentiation (chondrogenic differentiation) of EPCs (Fig. S2).

The chondrogenic differentiation of endothelial cells has been identified in vascular calcification and heterotopic ossification [10,11,38]. However, studies have focused on changes in endothelial cells, disregarding the potential contribution of EPCs. In addition to their role in pathological processes, EPCs are known to participate in tissue repair and regeneration. In the current study, we demonstrated that EPCs could transform into stem cells (tEPCs) through EndMT (Figs. S1 and S2) and differentiate into chondrocyte-like cells (CEPCs) via chondrogenic induction *in vitro*. Compared with EPCs, CEPCs exhibited increased *Col II*, *ACAN*, and *SOX9* expression, expressed chondrocyte surface markers,

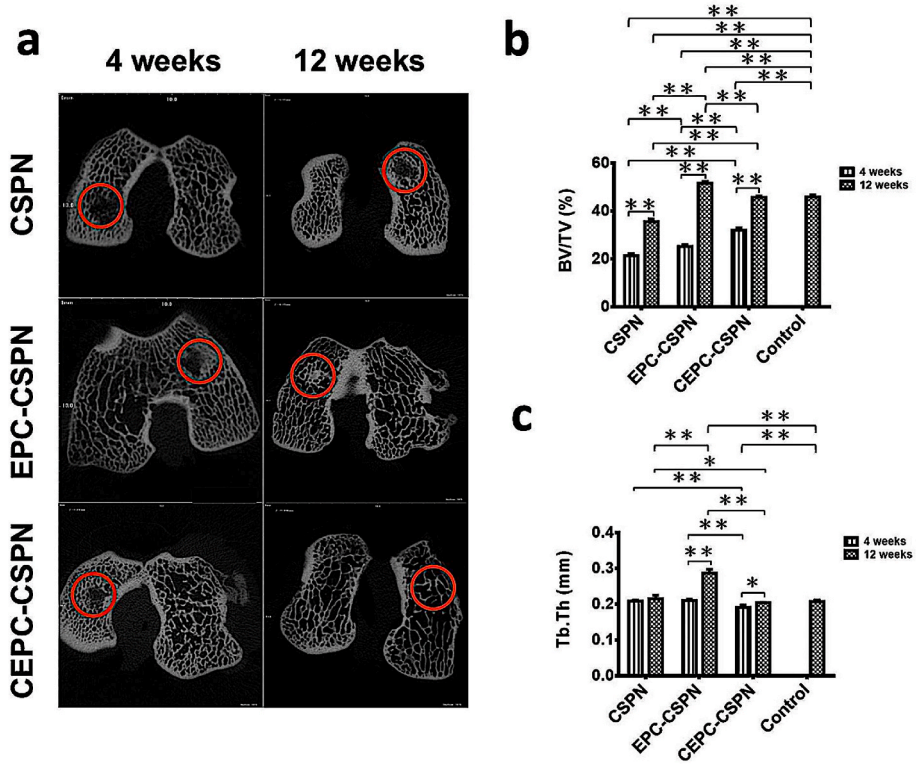

Fig. 8. Using CEPCs induces an effective and rapid improvement in bone remodeling. (**a**) Two-dimensional (2D) micro-computed tomography images in the frontal plane for bone assessment, with red circles indicating the defect sites. (**b**) BV/TV. (**c**) Tb.Th. The reported values are the average of $n = 6 \pm$ standard deviation. $^{*}P < 0.05$ and $^{**}P < 0.01$. Abbreviations: BV/TV, the ratio of bone volume to tissue volume; Tb.Th, thickness of trabecular bone; CSPN, chitosan-graft-poly (N-isopropylacrylamide); EPC-CSPN, CSPN scaffold containing endothelial progenitor cells; CEPC-CSPN, CSPN scaffold containing chondrogenic endothelial progenitor cells.

and secreted cartilage-specific matrix components. The addition of growth factors to the cell differentiation induction medium led to an increase in *Col I* expression in the CEPC group. A previous study [39] has reported enhanced *Col I* expression in MSCs exposed to exogenous growth factors. We subsequently evaluated the chondrogenic potential of tEPCs in co-culture systems with chondrocytes. Compared with monocultures, tEPCs co-cultured with chondrocytes underwent chondrocyte proliferation (Fig. S3), chondrogenic differentiation, and enhanced cartilage-specific matrix production (Figs. S4 and S5). These findings suggest that chondrocytes release soluble factors that induce the chondrogenic differentiation of tEPCs and that tEPC-released paracrine factors stimulate chondrocyte proliferation, consistent with previous reports [40,41].

Additionally, previous studies demonstrated that compressive strain also plays a central role in chondrogenic differentiation [42,43]. Mechanical cues significantly influence ECM synthesis in chondrocytes and play an important role in the differentiation of MSCs. In the present study, we also investigated the effect of dynamic mechanical compression on the chondrogenic differentiation of CEPCs in three-dimensional (3D)-printed CSPN scaffolds. Our results showed that the dynamic compression loading group enhanced the synthesis of the cartilage matrix of CEPCs in 3D-printed CSPN scaffolds compared with the unloaded control group after 21 days of culture (Fig. S6). Our findings suggest that the CEPC-seeded CSPN hydrogel inks can allow direct 3D printing into complex constructs, and the superior chondrogenic capacity of CEPCs in 3D-printed CSPN scaffolds can be promoted and maintained with compression loading. Furthermore, these data also mean that 3D-printed CEPC-CSPN scaffolds are easy to fabricate and can enhance the chondroprotective effect of the scaffolds through normal physical stimulation. This approach gives a new insight into the applications of cell-based clinical treatments for cartilage replacement and regeneration.

Cell-derived exosomes may also play a role in cartilage regeneration [44]. In the current study, tEPC-derived exosomes enhanced the proliferation of senescent periarticular stem cells (Fig. S7), suggesting that tEPCs promote the growth, proliferation, and differentiation of mature chondrocytes and stem/progenitor cells in the knee joint (Figs. S3 and S7). This finding also supports the role of tEPC-derived CEPCs in cartilage repair. In this study, we also showed that CEPC-CSPNs exhibited increased cell aggregation and enhanced tissue-specific ECM deposition after 28 days compared with EPC-CSPNs (Fig. S8). The chondrogenic differentiation of EPCs (CEPC-CSPNs) had a positive effect on the regeneration of hyaline cartilage *in vivo*, as evidenced by the presence of columnar rounded chondrocytes and elevated levels of Col II and sGAG in the repair tissue, compared with undifferentiated EPCs (EPC-CSPNs) and CSPNs (scaffold only). Our *in vivo* results also demonstrated that the expression of chondrogenesis markers in the cells in the regenerative tissue of the cartilage layer was increased in the CEPC-CSPN group compared with EPC-CSPN and CSPN-only groups (Fig. S9). Based on these findings, the primary source of stem/progenitor cells in the bone marrow during cartilage regeneration includes both bone marrow-derived MSCs and EPCs, which possess robust regenerative potential and can influence cartilage repair through their chondrogenic potential.

Biomaterial scaffolds used for cartilage tissue engineering should be biodegradable and possess physical structures and chemical compositions similar to the cartilage matrix. Chitosan is an ideal bioactive material owing to its biodegradable and non-toxic properties. The structure of chitosan closely resembles that of GAG, a major component of the articular cartilage ECM. Chitosan, as a GAG analog, is a favorable choice for fabricating scaffolds to repair OCDs. Previous studies [45,46] have demonstrated the superior regenerative potential of chitosan-based

scaffolds in the regeneration of the chondral layer of OCDs. However, the effects of chitosan-based scaffolds on the subchondral bone layer of OCDs remain unexplored. In this study, the CSPN scaffold not only exhibited regenerative effects on the chondral layer of OCDs but also demonstrated repair capacity for the subchondral bone layer, although it was less effective than the EPC-CSPN and CEPC-CSPN scaffolds. Chitosan is an attractive bone scaffold material because of its ability to support osteoblast attachment and proliferation, along with mineralized bone matrix formation *in vitro* [47]. Modified chitosan scaffolds exhibit osteoconductivity in surgical bone defects [48]. Therefore, chitosan has emerged as a promising biomaterial for bone tissue engineering.

In addition, chitosan is a suitable biopolymer for nanomaterial synthesis [49]. However, the traditional method of nanomaterial synthesis has several problems, such as the production of toxic waste and the consumption of a large amount of energy. Therefore, green nanotechnology has been proposed as a new approach to synthesizing nanomaterials. In the biosynthesis procedure for synthesizing green nanomaterials, microorganisms, biodegradable polymers, and plant extracts [50,51] can act as reductants and capping agents [52]. The CSPN scaffold with food-grade chitosan is a desirable biodegradable polymer that is easy to fabricate [24] and may act as an auxiliary agent to synthesize a novel green nanomaterial for cartilage regeneration.

Polymer-based tissue engineering scaffolds are frequently combined with bioactive factors to yield bioactive composite scaffolds [53–57]. MSCs can facilitate bone regeneration by differentiating into osteoblasts or secreting trophic factors that promote osteogenic activity [58]. Herein, we characterized EndMT-derived cells, demonstrating their similarity to MSCs in terms of morphology, surface markers, self-renewal, and multipotency. Herein, EndMT-derived cells were induced to differentiate into chondrocyte-like cells. They were combined with chitosan-based scaffolds, enhancing the expression of osteogenic markers in cells in the regenerative tissue of the subchondral bone layer and promoting subchondral bone regeneration (Fig. S9). These findings suggest that chondrocyte-like cells promote regeneration by undergoing terminal differentiation or transdifferentiation into osteoblasts, as previously reported [59,60]. Chondrocyte-like cells induce osteogenic differentiation of MSCs to promote osteoid matrix formation [61], confirming their role in bone regeneration.

Cell therapy involves replacing deficient/absent cells with healthy ones, thus introducing the concept of "living medicines." However, transplantation has limitations, including limited retention and inferior engraftment. To overcome these challenges, injectable thermoresponsive hydrogels have been employed as cell carriers in regenerative medicine. The CSPN hydrogel used in the current study can be homogeneously mixed with cells (**Video S2** and **S3**), allowing minimally invasive transplantation via injection. The CSPN hydrogel rapidly forms after injection (**Video S1**), preventing the undesirable diffusion of gel precursors and cells into surrounding tissues. This makes it an ideal vehicle for delivering cells to OCDs. Modified poly (*N*-isopropylacrylamide) hydrogels can facilitate cell encapsulation, improve cell chondrogenesis, and promote cartilage tissue formation for cartilage regeneration [23,62]. However, most studies for cartilage repair have focused on the regenerative potential of tissue-derived stem cells encapsulated in CSPN scaffolds. Unlike previous studies [24–26], the present study reported the induction of osteochondral tissue regeneration in rabbits via the transplantation of a biocomposite CSPN construct combined with CEPCs. In contrast to the conventional surgical treatment and MSC-based therapy, the approach employed in this study for cartilage repair can replace open implants with minimally invasive injections, have fewer complications, shorter hospital stays, be used to form any desired shape *in situ* to match irregular defects, avoid adult tissue harvesting, and reduce the occurrence of cell phenotype change because of cell passages and culture conditions *in vitro*; hence, it can be considered an alternative source of treatment strategies for cartilage defect regeneration. However, a limitation of our study is the absence of a biomechanical test to measure the mechanical properties of the regenerated cartilage and the surface friction coefficient. To minimize the number of sacrificed animals, we focused on the degree of regeneration and biochemical and molecular matrix analyses. Further investigation is warranted, including the comparison of CSPNs with MSCs and chondrocytes, weight-bearing *versus* non-weight-bearing articulations, and preclinical studies and clinical trials.

Supplementary video related to this article can be found at https://doi.org/10.1016/j.mtbio.2024.101174

5. Conclusions

LEPCs undergo TGF-β1-induced EndMT to become tEPCs, which exhibit superior chondrogenic potential *in vitro* and may serve as an alternative cell source for cartilage tissue engineering. Our study demonstrated the feasibility of repairing the articular cartilage using a biocomposite CSPN scaffold. Osteochondral regeneration can be enhanced through CEPC application. Although EPCs are typically used for vascular regeneration, we highlight the synergistic effects of implanting a biocomposite CSPN scaffold combined with CEPCs on osteochondral regeneration, even without mature MSCs/differentiated cells. CEPC-CSPNs promoted the formation of neo-hyaline cartilage with subchondral bone that integrated with surrounding host bone. In contrast to traditional approaches, this implant, combined with an intraarticular injection system, is a straightforward approach to osteochondral regeneration. This bioactive cellular transport system holds promise for innovative therapeutic strategies in cartilage regenerative medicine.

Funding

This study was supported by grants from the National Science and Technology Council of Taiwan (NSTC 110-2314-B-006-101, 101-2221-E-006-062-MY3, and 111-2740-B-006-002).

CRediT authorship contribution statement

Tzu-Hsiang Lin: Writing – original draft, Validation, Methodology, Investigation, Data curation, Conceptualization. **Hsueh-Chun Wang:** Validation, Resources, Methodology, Funding acquisition, Formal analysis. **Yau-Lin Tseng:** Supervision, Resources, Methodology, Funding acquisition, Formal analysis. **Ming-Long Yeh:** Writing – review & editing, Supervision, Resources, Project administration, Formal analysis, Conceptualization.

Declaration of competing interest

The authors declare that they have no known competing financial interests or personal relationships that could have appeared to influence the work reported in this paper.

Data availability

Data will be made available on request.

Acknowledgements

We are grateful for the technical services provided by the Bioimaging Core Facility of the National Core Facility for Biopharmaceuticals, National Science and Technology Council, Taiwan.

Appendix A. Supplementary data

Supplementary data to this article can be found online at https://doi.org/10.1016/j.mtbio.2024.101174.

References

[1] R. Katayama, S. Wakitani, N. Tsumaki, Y. Morita, I. Matsushita, R. Gejo, T. Kimura, Repair of articular cartilage defects in rabbits using CDMP1 gene-transfected autologous mesenchymal cells derived from bone marrow, Rheumatology 43 (2004) 980–985, https://doi.org/10.1093/rheumatology/keh240.

[2] J.D. Kretlow, Y.Q. Jin, W. Liu, W.J. Zhang, T.H. Hong, G. Zhou, L.S. Baggett, A. G. Mikos, Y. Cao, Donor age and cell passage affects differentiation potential of murine bone marrow-derived stem cells, BMC Cell Biol. 9 (2008) 60, https://doi.org/10.1186/1471-2121-9-60.

[3] M.R. Homicz, B.L. Schumacher, R.L. Sah, D. Watson, Effects of serial expansion of septal chondrocytes on tissue-engineered neocartilage composition, Otolaryngol. Head Neck Surg. 127 (2002) 398–408, https://doi.org/10.1067/mhn.2002.129730.

[4] H.C. Wang, T.H. Lin, N.J. Chang, H.C. Hsu, M.L. Yeh, Continuous passive motion promotes and maintains chondrogenesis in autologous endothelial progenitor cell-loaded porous PLGA scaffolds during osteochondral defect repair in a rabbit model, Int. J. Mol. Sci. 20 (2019), https://doi.org/10.3390/ijms20020259.

[5] J. Hur, C.H. Yoon, H.S. Kim, J.H. Choi, H.J. Kang, K.K. Hwang, B.H. Oh, M.M. Lee, Y.B. Park, Characterization of two types of endothelial progenitor cells and their different contributions to neovasculogenesis, Arterioscler. Thromb. Vasc. Biol. 24 (2004) 288–293, https://doi.org/10.1161/01.atv.0000114236.77009.06.

[6] A.R. Chade, X. Zhu, R. Lavi, J.D. Krier, S. Pislaru, R.D. Simari, C. Napoli, A. Lerman, L.O. Lerman, Endothelial progenitor cells restore renal function in chronic experimental renovascular disease, Circulation 119 (2009) 547–557, https://doi.org/10.1161/circulationaha.108.788653.

[7] N.J. Chang, C.F. Lam, C.C. Lin, W.L. Chen, C.F. Li, Y.T. Lin, M.L. Yeh, Transplantation of autologous endothelial progenitor cells in porous PLGA scaffolds create a microenvironment for the regeneration of hyaline cartilage in rabbits, Osteoarthritis Cartilage 21 (2013) 1613–1622, https://doi.org/10.1016/j.joca.2013.07.016.

[8] D. Medici, R. Kalluri, Endothelial-mesenchymal transition and its contribution to the emergence of stem cell phenotype, Semin. Cancer Biol. 22 (2012) 379–384, https://doi.org/10.1016/j.semcancer.2012.04.004.

[9] D. Medici, Endothelial-mesenchymal transition in regenerative medicine, Stem Cell. Int. 2016 (2016) 6962801, https://doi.org/10.1155/2016/6962801.

[10] D. Medici, E.M. Shore, V.Y. Lounev, F.S. Kaplan, R. Kalluri, B.R. Olsen, Conversion of vascular endothelial cells into multipotent stem-like cells, Nat. Med. 16 (2010) 1400–1406, https://doi.org/10.1038/nm.2252.

[11] D. Medici, B.R. Olsen, The role of endothelial-mesenchymal transition in heterotopic ossification, J. Bone Miner. Res. 27 (2012) 1619–1622, https://doi.org/10.1002/jbmr.1691.

[12] L.A. van Meeteren, P. ten Dijke, Regulation of endothelial cell plasticity by TGF-beta, Cell Tissue Res. 347 (2012) 177–186, https://doi.org/10.1007/s00441-011-1222-6.

[13] A.M. Freyria, F. Mallein-Gerin, Chondrocytes or adult stem cells for cartilage repair: the indisputable role of growth factors, Injury 43 (2012) 259–265, https://doi.org/10.1016/j.injury.2011.05.035.

[14] M.P. Verdier, S. Seite, K. Guntzer, J.P. Pujol, K. Boumediene, Immunohistochemical analysis of transforming growth factor beta isoforms and their receptors in human cartilage from normal and osteoarthritic femoral heads, Rheumatol. Int. 25 (2005) 118–124, https://doi.org/10.1007/s00296-003-0409-x.

[15] W. Ge, Y. Mi, S. Xu, T. Li, Y. Lu, J. Jiang, rhBMP-7 suppresses TGF-β1-induced endothelial to mesenchymal transition in circulating endothelial cells by regulating Smad5, Mol. Med. Rep. 21 (2020) 478–484, https://doi.org/10.3892/mmr.2019.10842.

[16] A.K. Ghosh, V. Nagpal, J.W. Covington, M.A. Michaels, D.E. Vaughan, Molecular basis of cardiac endothelial-to-mesenchymal transition (EndMT): differential expression of microRNAs during EndMT, Cell. Signal. 24 (2012) 1031–1036, https://doi.org/10.1016/j.cellsig.2011.12.024.

[17] D.M. Gonzalez, D. Medici, Signaling mechanisms of the epithelial-mesenchymal transition, Sci. Signal. 7 (2014) re8, https://doi.org/10.1126/scisignal.2005189.

[18] J.R. Moonen, G. Krenning, M.G. Brinker, J.A. Koerts, M.J. van Luyn, M.C. Harmsen, Endothelial progenitor cells give rise to pro-angiogenic smooth muscle-like progeny, Cardiovasc. Res. 86 (2010) 506–515, https://doi.org/10.1093/cvr/cvq012.

[19] M.J. Susienka, D. Medici, Vascular endothelium as a novel source of stem cells for bioengineering, Biomatter 3 (2013) e24647, https://doi.org/10.4161/biom.24647.

[20] S.B. Lee, D.I. Ha, S.K. Cho, S.J. Kim, Y.M. Lee, Temperature/pH-sensitive comb-type graft hydrogels composed of chitosan and poly(N-isopropylacrylamide), J. Appl. Polym. Sci. 92 (2004) 2612–2620, https://doi.org/10.1002/app.20265.

[21] J.K. Suh, H.W. Matthew, Application of chitosan-based polysaccharide biomaterials in cartilage tissue engineering: a review, Biomaterials 21 (2000) 2589–2598, https://doi.org/10.1016/s0142-9612(00)00126-5.

[22] J.P. Chen, T.H. Cheng, Thermo-responsive chitosan-graft-poly(N-isopropylacrylamide) injectable hydrogel for cultivation of chondrocytes and meniscus cells, Macromol. Biosci. 6 (2006) 1026–1039, https://doi.org/10.1002/mabi.200600142.

[23] J.H. Cho, S.H. Kim, K.D. Park, M.C. Jung, W.I. Yang, S.W. Han, J.Y. Noh, J.W. Lee, Chondrogenic differentiation of human mesenchymal stem cells using a thermosensitive poly(N-isopropylacrylamide) and water-soluble chitosan copolymer, Biomaterials 25 (2004) 5743–5751, https://doi.org/10.1016/j.biomaterials.2004.01.051.

[24] T.-H. Lin, H.-C. Wang, M.-C. Wu, H.-C. Hsu, M.-L. Yeh, A bilineage thermosensitive hydrogel system for stimulation of mesenchymal stem cell differentiation and enhancement of osteochondral regeneration, Composites, Part B (2022) 109614, https://doi.org/10.1016/j.compositesb.2022.109614.

[25] A. Mellati, M.V. Kiamahalleh, S.H. Madani, S. Dai, J. Bi, B. Jin, H. Zhang, Poly(N-isopropylacrylamide) hydrogel/chitosan scaffold hybrid for three-dimensional stem cell culture and cartilage tissue engineering, J. Biomed. Mater. Res., Part A 104 (2016) 2764–2774, https://doi.org/10.1002/jbm.a.35810.

[26] S.W. Wu, X. Liu, A.L. Miller 2nd, Y.S. Cheng, M.L. Yeh, L. Lu, Strengthening injectable thermo-sensitive NIPAAm-g-chitosan hydrogels using chemical cross-linking of disulfide bonds as scaffolds for tissue engineering, Carbohydr. Polym. 192 (2018) 308–316, https://doi.org/10.1016/j.carbpol.2018.03.047.

[27] C.F. Lam, Y.C. Liu, J.K. Hsu, P.A. Yeh, T.Y. Su, C.C. Huang, M.W. Lin, P.C. Wu, P. J. Chang, Y.C. Tsai, Autologous transplantation of endothelial progenitor cells attenuates acute lung injury in rabbits, Anesthesiology 108 (2008) 392–401, https://doi.org/10.1097/ALN.0b013e318164ca64.

[28] S.C. Wu, J.K. Chang, C.K. Wang, G.J. Wang, M.L. Ho, Enhancement of chondrogenesis of human adipose derived stem cells in a hyaluronan-enriched microenvironment, Biomaterials 31 (2010) 631–640, https://doi.org/10.1016/j.biomaterials.2009.09.089.

[29] Y.W. Eom, J.E. Lee, M.S. Yang, I.K. Jang, H.E. Kim, D.H. Lee, Y.J. Kim, W.J. Park, J. H. Kong, K.Y. Shim, J.I. Lee, H.S. Kim, Rapid isolation of adipose tissue-derived stem cells by the storage of lipoaspirates, Yonsei Med. J. 52 (2011) 999–1007, https://doi.org/10.3349/ymj.2011.52.6.999.

[30] R.W. Farndale, D.J. Buttle, A.J. Barrett, Improved quantitation and discrimination of sulphated glycosaminoglycans by use of dimethylmethylene blue, Biochim. Biophys. Acta 883 (1986) 173–177, https://doi.org/10.1016/0304-4165(86)90306-5.

[31] T. He, L.A. Smith, S. Harrington, K.A. Nath, N.M. Caplice, Z.S. Katusic, Transplantation of circulating endothelial progenitor cells restores endothelial function of denuded rabbit carotid arteries, Stroke 35 (2004) 2378–2384, https://doi.org/10.1161/01.STR.0000141893.33677.5d.

[32] C.T. Hung, E.G. Lima, R.L. Mauck, E. Takai, M.A. LeRoux, H.H. Lu, R.G. Stark, X. E. Guo, G.A. Ateshian, Anatomically shaped osteochondral constructs for articular cartilage repair, J. Biomech. 36 (2003) 1853–1864, https://doi.org/10.1016/s0021-9290(03)00213-6.

[33] N.J. Chang, C.C. Lin, C.F. Li, D.A. Wang, N. Issariyaku, M.L. Yeh, The combined effects of continuous passive motion treatment and acellular PLGA implants on osteochondral regeneration in the rabbit, Biomaterials 33 (2012) 3153–3163, https://doi.org/10.1016/j.biomaterials.2011.12.054.

[34] T. Asahara, T. Murohara, A. Sullivan, M. Silver, R. van der Zee, T. Li, B. Witzenbichler, G. Schatteman, J.M. Isner, Isolation of putative progenitor endothelial cells for angiogenesis, Science 275 (1997) 964–967, https://doi.org/10.1126/science.275.5302.964.

[35] S. Piera-Velazquez, F.A. Mendoza, S.A. Jimenez, Endothelial to mesenchymal transition (EndoMT) in the pathogenesis of human fibrotic diseases, J. Clin. Med. 5 (2016), https://doi.org/10.3390/jcm5040045.

[36] D. Medici, S. Potenta, R. Kalluri, Transforming growth factor-beta2 promotes Snail-mediated endothelial-mesenchymal transition through convergence of Smad-dependent and Smad-independent signalling, Biochem. J. 437 (2011) 515–520, https://doi.org/10.1042/BJ20101500.

[37] Y. Xiang, Y. Zhang, Y. Tang, Q. Li, MALAT1 modulates TGF-beta1-induced endothelial-to-mesenchymal transition through downregulation of miR-145, Cell. Physiol. Biochem. 42 (2017) 357–372, https://doi.org/10.1159/000477479.

[38] R. Tang, M. Gao, M. Wu, H. Liu, X. Zhang, B. Liu, High glucose mediates endothelial-to-chondrocyte transition in human aortic endothelial cells, Cardiovasc. Diabetol. 11 (2012) 113, https://doi.org/10.1186/1475-2840-11-113.

[39] N. Indrawattana, G. Chen, M. Tadokoro, L.H. Shann, H. Ohgushi, T. Tateishi, J. Tanaka, A. Bunyaratvej, Growth factor combination for chondrogenic induction from human mesenchymal stem cell, Biochem. Biophys. Res. Commun. 320 (2004) 914–919, https://doi.org/10.1016/j.bbrc.2004.06.029.

[40] L. Xu, Y. Wu, Z. Xiong, Y. Zhou, Z. Ye, W.-S. Tan, Mesenchymal stem cells reshape and provoke proliferation of articular chondrocytes by paracrine secretion, Sci. Rep. 6 (2016) 32705, https://doi.org/10.1038/srep32705.

[41] J. Shi, J. Liang, B. Guo, Y. Zhang, Q. Hui, P. Chang, K. Tao, Adipose-derived stem cells cocultured with chondrocytes promote the proliferation of chondrocytes, Stem Cells Int. 2017 (2017) 1709582, https://doi.org/10.1155/2017/1709582, 1709582.

[42] Y. Ge, Y. Li, Z. Wang, L. Li, H. Teng, Q. Jiang, Effects of mechanical compression on chondrogenesis of human synovium-derived mesenchymal stem cells in agarose hydrogel, Front. Bioeng. Biotechnol. 9 (2021) 697281, https://doi.org/10.3389/fbioe.2021.697281.

[43] M.J. Zuscik, M.J. Hilton, X. Zhang, D. Chen, R.J. O'Keefe, Regulation of chondrogenesis and chondrocyte differentiation by stress, J. Clin. Invest. 118 (2008) 429–438, https://doi.org/10.1172/jci34174.

[44] S. Zhang, W.C. Chu, R.C. Lai, S.K. Lim, J.H. Hui, W.S. Toh, Exosomes derived from human embryonic mesenchymal stem cells promote osteochondral regeneration, Osteoarthritis Cartilage 24 (2016) 2135–2140, https://doi.org/10.1016/j.joca.2016.06.022.

[45] K. Zhang, Y. Zhang, S. Yan, L. Gong, J. Wang, X. Chen, L. Cui, J. Yin, Repair of an articular cartilage defect using adipose-derived stem cells loaded on a polyelectrolyte complex scaffold based on poly(l-glutamic acid) and chitosan, Acta Biomater. 9 (2013) 7276–7288, https://doi.org/10.1016/j.actbio.2013.03.025.

[46] M. Zhao, Z. Chen, K. Liu, Y.Q. Wan, X.D. Li, X.W. Luo, Y.G. Bai, Z.L. Yang, G. Feng, Repair of articular cartilage defects in rabbits through tissue-engineered cartilage constructed with chitosan hydrogel and chondrocytes, J. Zhejiang Univ. - Sci. B 16 (2015) 914–923, https://doi.org/10.1631/jzus.B1500036.

[47] Y.J. Seol, J.Y. Lee, Y.J. Park, Y.M. Lee, K. Young, I.C. Rhyu, S.J. Lee, S.B. Han, C. P. Chung, Chitosan sponges as tissue engineering scaffolds for bone formation, Biotechnol. Lett. 26 (2004) 1037–1041, https://doi.org/10.1023/B:BILE.0000032962.79531.fd.

[48] R.A. Muzzarelli, M. Mattioli-Belmonte, C. Tietz, R. Biagini, G. Ferioli, M. A. Brunelli, M. Fini, R. Giardino, P. Ilari, G. Biagini, Stimulatory effect on bone formation exerted by a modified chitosan, Biomaterials 15 (1994) 1075–1081.

[49] L. Luo, L. Zhu, Y. Xu, L. Shen, X. Wang, Y. Ding, Q. Li, D. Deng, Hydrogen peroxide biosensor based on horseradish peroxidase immobilized on chitosan-wrapped NiFe2O4 nanoparticles, Microchim. Acta 174 (2011) 55–61, https://doi.org/10.1007/s00604-011-0591-6.

[50] M. Karadağ, S. Doğan, Mask for moisturizing skin and body made from cold-pressed paste of peanuts (Arachis hypogaea L.), ABES 9 (2024) 155–160, https://doi.org/10.62476/abes9155.

[51] M. Karadağ, S. Omarova, Use of Prunus armeniaca L. seed oil and pulp in health and cosmetic products, ABES 9 (2024) 105–110, https://doi.org/10.62476/abess105.

[52] O.V. Kharissova, H.V.R. Dias, B.I. Kharisov, B.O. Pérez, V.M.J. Pérez, The greener synthesis of nanoparticles, Trends Biotechnol. 31 (2013) 240–248, https://doi.org/10.1016/j.tibtech.2013.01.003.

[53] C. Gao, W. Dai, X. Wang, L. Zhang, Y. Wang, Y. Huang, Z. Yuan, X. Zhang, Y. Yu, X. Yang, Q. Cai, Magnesium gradient-based hierarchical scaffold for dual-lineage regeneration of osteochondral defect, Adv. Funct. Mater. 33 (2023) 2304829, https://doi.org/10.1002/adfm.202304829.

[54] L. Zhang, W. Dai, C. Gao, W. Wei, R. Huang, X. Zhang, Y. Yu, X. Yang, Q. Cai, Multileveled hierarchical hydrogel with continuous biophysical and biochemical gradients for enhanced repair of full-thickness osteochondral defect, Adv. Mater. 35 (2023) 2209565, https://doi.org/10.1002/adma.202209565.

[55] X. Wang, W. Dai, C. Gao, L. Zhang, Z. Wan, T. Zhang, Y. Wang, Y. Tang, Y. Yu, X. Yang, Q. Cai, Spatiotemporal modulated scaffold for endogenous bone regeneration via harnessing sequentially released guiding signals, ACS Appl. Mater. Interfaces 15 (2023) 58873–58887, https://doi.org/10.1021/acsami.3c13963.

[56] S. Shahi, F. Dehghani, E.D. Abdolahinia, S. Sharifi, E. Ahmadian, M. Gajdács, K. Kárpáti, S.M. Dizaj, A. Eftekhari, T. Kavetskyy, Effect of gelatinous spongy scaffold containing nano-hydroxyapatite on the induction of odontogenic activity of dental pulp stem cells, J. King Saud Univ. Sci. 34 (2022) 102340, https://doi.org/10.1016/j.jksus.2022.102340.

[57] P. Salahshour, S. Abdolmaleki, S. Monemizadeh, S. Gholizadeh, S. Khaksar, Nanobiomaterials/bioinks based scaffolds in 3D bioprinting for tissue engineering and artificial human organs, ABES 9 (2024) 97–104.

[58] H. Liu, H. Peng, Y. Wu, C. Zhang, Y. Cai, G. Xu, Q. Li, X. Chen, J. Ji, Y. Zhang, H. W. OuYang, The promotion of bone regeneration by nanofibrous hydroxyapatite/chitosan scaffolds by effects on integrin-BMP/Smad signaling pathway in BMSCs, Biomaterials 34 (2013) 4404–4417, https://doi.org/10.1016/j.biomaterials.2013.02.048.

[59] F. Descalzi Cancedda, C. Gentili, P. Manduca, R. Cancedda, Hypertrophic chondrocytes undergo further differentiation in culture, J. Cell Biol. 117 (1992) 427–435, https://doi.org/10.1083/jcb.117.2.427.

[60] X. Zhou, K. von der Mark, S. Henry, W. Norton, H. Adams, B. de Crombrugghe, Chondrocytes transdifferentiate into osteoblasts in endochondral bone during development, postnatal growth and fracture healing in mice, PLoS Genet. 10 (2014) e1004820, https://doi.org/10.1371/journal.pgen.1004820.

[61] N.S. Hwang, S. Varghese, C. Puleo, Z. Zhang, J. Elisseeff, Morphogenetic signals from chondrocytes promote chondrogenic and osteogenic differentiation of mesenchymal stem cells, J. Cell. Physiol. 212 (2007) 281–284, https://doi.org/10.1002/jcp.21052.

[62] H. Sa-Lima, K. Tuzlakoglu, J.F. Mano, R.L. Reis, Thermoresponsive poly(N-isopropylacrylamide)-g-methylcellulose hydrogel as a three-dimensional extracellular matrix for cartilage-engineered applications, J. Biomed. Mater. Res., Part A 98 (2011) 596–603, https://doi.org/10.1002/jbm.a.33140.